Journal of *Marine Science and Engineering*

MDPI

Article

Adaptive Distributed Heterogeneous Formation Control for UAV-USVs with Input Quantization

Jun Ning [1], Yuyang Huang [2], Zihan Liu [1], Wei Li [1,*] and Xingwang Yue [1]

[1] College of Navigation, Dalian Maritime University, Dalian 116026, China; junning@dlmu.edu.cn (J.N.); han15645746622@dlmu.edu.cn (Z.L.); dmuyxw@dlmu.edu.cn (X.Y.)
[2] School of Instrumentation Science and Engineering, Harbin Institute of Technology, Harbin 150001, China; huangyuyang@dlmu.edu.cn
* Correspondence: li_wei@dlmu.edu.cn

Abstract: This paper investigates the cooperative formation trajectory tracking problem for heterogeneous unmanned aerial vehicle (UAV) and multiple unmanned surface vessel (USV) systems with input quantization performance. Firstly, at the kinematic level, a distributed guidance law based on an extended state observer (ESO) is designed to compensate for the unknown speed of neighbor agents for expected trajectory tracking, and subsequently at the dynamic level, an ESO is utilized to estimate model uncertainties and environmental disturbances. Following that, a linear analytic model is employed to depict the input quantization process, and the corresponding adaptive quantization controller is designed without necessitating prior information on quantization parameters. Based on the input-to-state stability, the stability of the proposed control structure is proved, and all the signals in the closed-loop system are ultimately bounded. Finally, a simulation study is provided to show the efficacy of the proposed strategy.

Keywords: heterogeneous formation control system; UAV-USVs; extended state observer; input quantization; sliding mode control

check for updates

Citation: Ning, J.; Huang, Y.; Liu, Z.; Li, W.; Yue, X. Adaptive Distributed Heterogeneous Formation Control for UAV-USVs with Input Quantization. *J. Mar. Sci. Eng.* **2024**, *12*, 975. https://doi.org/10.3390/jmse12060975

Academic Editor: Mohamed Benbouzid

Received: 25 April 2024
Revised: 1 June 2024
Accepted: 7 June 2024
Published: 11 June 2024

Copyright: © 2024 by the authors. Licensee MDPI, Basel, Switzerland. This article is an open access article distributed under the terms and conditions of the Creative Commons Attribution (CC BY) license (https://creativecommons.org/licenses/by/4.0/).

1. Introduction

In recent times, owing to escalating societal demands, there has been a significant advancement in the development of unmanned systems [1–3]. These systems offer benefits such as compactness, agility, affordability, and the elimination of casualty risks [4–6]. They can operate in hazardous zones or areas unsuitable for manned vehicles, broaden operational possibilities, and are cost effective [7,8]. To further enhance the operational efficiency of these unmanned systems, the focus on formation strategies in unmanned systems has gained prominence in practical engineering applications [9,10].

The application of unmanned surface vehicles (USVs) in ocean engineering has expanded significantly, which can be attributed to their advantages such as an enhanced load capacity, greater operational convenience, and reduced cost of missions [11]. Nevertheless, the limited observational range of USVs poses challenges in locating targets during maritime search and rescue operations [12]. To address this limitation, integrating unmanned aerial vehicles (UAVs) with USV systems to form heterogeneous multi-agent systems has proven beneficial [13]. A USV supplemented by the agility of a UAV and its superior target search capabilities effectively broadens the communication scope at sea among USVs, thereby expanding the operational area of these heterogeneous systems [14,15]. Therefore, exploring the formation dynamics within these heterogeneous systems holds substantial importance in engineering.

Significant advancements in the cooperative tracking control of UAVs and USVs have been made, with notable methodologies including the leader–follower method [16], virtual structure method [17], behavior-based approach [18], and model prediction method [19]. Kai Xue [20] proposes a distributed collaborative tracking method based on leader–follower

for a heterogeneous multi-agent system composed of UAVs and multiple USVs. Haitao Liu [21] proposes a distributed formation control protocol for UAV-USV heterogeneous systems to ensure that the target trajectory is tracked within a fixed time and a predetermined formation configuration is formed under various uncertainties. Shaoshi Li [22] proposes a formation control scheme based on velocity estimation, which only requires the relative azimuth vector between adjacent aircraft to achieve the desired formation. Dapeng Huang [19] proposes a distributed model predictive formation control algorithm for heterogeneous multi-agent systems based on directed topology, which realizes the coordination of heterogeneous formation between multiple UAVs and USVs. In literature [23], a global fixed-time adaptive neural network non-singular fast terminal sliding formation controller is designed to ensure that the trajectory of the target is tracked within a fixed time and a predetermined formation configuration is formed. Huiyan Li [24] designed a linear time-varying UAV-USV system based on distributed control, proposed the necessary conditions to maintain the consistency of the system, and expounded the effects of inertia matrix parameters and the heterogeneity between UAVs and USVs on the controller performance. The collective research efforts of these scholars have paved the way for enhanced understanding and practical implementation of heterogeneous multi-agent formation and control within the realm of UAVs and USVs.

Nonetheless, it is worth noting that the aforementioned scholarly works have yet to address the intricate challenge posed by the constrained maritime communication bandwidth. For navigational tasks, the transfer of data among sensor components is dependent on the use of communication channels. Consequently, this requires the information to be quantized and encoded before its transmission. Moreover, in light of the channel bandwidth constraints, maintaining a seamless system functioning within the defined bandwidth limits necessitates incorporating quantization technologies. The application of these quantization methods enables a strategic decrease in communication frequency and effectively manages the number of controllers within a specific bandwidth range.

At present, some studies have considered the quantitative problems existing in the practice of physical systems [25–33]. However, the input quantization of heterogeneous UAV and USV formation control systems has not been considered in the literature.

Based on the above problems, this paper designs the adaptive distributed heterogeneous formation control algorithm with input quantization. The research aims to advance cooperative tracking control strategies for UAV and USV formations, focusing on input quantization. This paper proposes an adaptive distributed heterogeneous formation control algorithm that incorporates input quantization to manage the constraints posed by limited communication bandwidth in maritime environments.

In contrast to the existing body of research, this paper stands out for the following salient attributes:

(1) Novelty in problem scope: Unlike prior studies [14,19–24,34–38], these research pioneers the exploration of the intricate domain concerning heterogeneous UAV and USV formation control coupled with input quantization. The integration of these two crucial factors is unprecedented in the field.

(2) Advanced estimation technique: Distinguishing itself from works such as [17,20,21,39–41], this paper leverages an extended state observer (ESO) methodology to assess the influence of external environmental factors deftly. Furthermore, it presents a strategic resolution to the challenges posed by heterogeneity by employing a unified model approach.

(3) Enhanced quantization methodology: In comparison to studies like [5,6,8,15,25–27,30–33], this paper introduces a unique approach to the quantization process. It elucidates this process via a linear time-varying model, which offers notable advantages. Most notably, it eliminates the need for explicit quantization parameter information, thus streamlining the implementation process.

The organization of this paper is as follows. Section 2 introduces some necessary preliminaries and states the problem formulation. Section 3 expounds on the controller

design. Section 4 provides the closed-loop system stability analysis. Section 5 demonstrates the simulation studies. Section 6 concludes the paper.

2. Problem Formulation

Consider a heterogeneous multi-agent system (HMAS) consisting of one leader UAV and N follower USVs. According to the results, in [42] the dynamic model of a quadrotor UAV can be described as

$$\begin{cases} \ddot{p}_{ax} = (\cos\phi\sin\theta\cos\psi + \sin\phi\sin\psi)\frac{u_p}{m_a} - \frac{d_x\dot{p}_{ax}}{m_a} + \Delta_{ax}, \\ \ddot{p}_{ay} = (\cos\phi\sin\theta\sin\psi + \sin\phi\cos\psi)\frac{u_p}{m_a} - \frac{d_y\dot{p}_{ay}}{m_a} + \Delta_{ay}, \\ \ddot{p}_{az} = (\cos\theta\cos\phi)\frac{u_p}{m_a} - \frac{d_z\dot{p}_{az}}{m_a} - g + \Delta_{az}, \end{cases} \tag{1}$$

$$\begin{cases} \ddot{\phi} = \dot{\theta}\dot{\psi}\frac{J_{ay}-J_{az}}{J_{ax}} - \frac{J_{ar}}{J_{ax}}\dot{\theta}\bar{d} + \frac{\tau_\phi}{J_{ax}} - \frac{d_\phi\dot{\phi}}{J_{ax}}, \\ \ddot{\theta} = \dot{\phi}\dot{\psi}\frac{J_{az}-J_{ax}}{J_{ay}} - \frac{J_{ar}}{J_{ay}}\dot{\phi}\bar{d} + \frac{\tau_\theta}{J_{ay}} - \frac{d_\theta\dot{\theta}}{J_{ay}}, \\ \ddot{\psi} = \dot{\phi}\dot{\theta}\frac{J_{ax}-J_{ay}}{J_{az}} + \frac{\tau_\psi}{J_{az}} - \frac{d_\psi\dot{\psi}}{J_{az}}, \end{cases} \tag{2}$$

where $[p_{ax}, p_{ay}, p_{az}]^T$ indicates the spatial location information of the UAV; $[\phi, \theta, \psi]^T$ indicates the attitude information of the UAV; u_p is defined as the control thrust of the UAV; $[\tau_\phi, \tau_\theta, \tau_\psi]^T$ indicates the three control torques of the UAV; m_a is the mass of the UAV; g indicates the gravitational acceleration; $\bar{d}$ indicates the overall residual rotor angle; $d_x, d_y, d_z, d_\phi, d_\theta, d_\psi$ denote the translational drag coefficients; J_{ax}, J_{ay}, J_{az} are the torques of the inertia; J_{ar} is the torque of the rotor's inertia; and $\Delta_{ax}, \Delta_{ay}, \Delta_{az}$ indicate the external interference encountered by the UAV.

Inspired by these results, considering external disturbances and parametric uncertainties, the three-degrees-of-freedom model of a UAV (1) can be redefined as follows:

$$\ddot{p}_a = g_a u_a + f_a + \Delta_a. \tag{3}$$

where $p_a = [p_{ax}, p_{ay}, p_{az}]^T$ denotes the position of the UAV, $f_a = [-d_x\dot{p}_{ax}/m_a, -d_y\dot{p}_{ay}/m_a, -d_z\dot{p}_{az}/m_a - g]^T$, $g_a = \mathrm{diag}\{1/m_a, 1/m_a, 1/m_a\}$, $\Delta_a = [\Delta_{ax}, \Delta_{ay}, \Delta_{az}]^T$, and $u_a = [u_{ax}, u_{ay}, u_{az}]^T$ is defined as

$$\begin{cases} u_{ax} = (\cos\phi\sin\theta\cos\psi + \sin\phi\sin\psi)u_p, \\ u_{ay} = (\cos\phi\sin\theta\sin\psi + \sin\phi\cos\psi)u_p, \\ u_{az} = (\cos\theta\cos\phi)u_p. \end{cases}$$

The kinematic and dynamic equation of the i-th USV in the XY plane is defined as [43]

$$\begin{cases} \dot{x}_{si} = \mu_{si}\cos\psi_{si} - v_{si}\sin\psi_{si}, \\ \dot{y}_{si} = \mu_{si}\sin\psi_{si} + v_{si}\cos\psi_{si}, \\ \dot{\psi}_{si} = r_{si}. \end{cases} \tag{4}$$

$$\begin{cases} \dot{\mu}_{si} = f_{\mu si}(\alpha_i) + \frac{1}{m_{\mu si}}\left(\tau^f_{\mu si} + w_{\mu si}\right), \\ \dot{v}_{si} = f_{vsi}(\alpha_i) + \frac{1}{m_{vsi}}w_{vsi}, \\ \dot{r}_{si} = f_{rsi}(\alpha_i) + \frac{1}{m_{rsi}}\left(\tau^f_{rsi} + w_{rsi}\right). \end{cases} \tag{5}$$

and

$$\begin{cases} f_{\mu si}(\alpha_i) = \dfrac{1}{m_{\mu si}}(m_{vsi}v_{si}r_{si} - d_{\mu si}\mu_{si} - d_{\mu si1}|\mu_{si}|\mu_{si}), \\ f_{vsi}(\alpha_i) = \dfrac{1}{m_{\mu si}}(-m_{\mu si}\mu_{si}r_{si} - d_{vsi}v_{si} - d_{vsi1}|v_{si}|v_{si}), \\ f_{rsi}(\alpha_i) = \dfrac{1}{m_{rsi}}((m_{\mu si} - m_{vsi})\mu_{si}v_{si} - d_{rsi}r_{si} - d_{rsi1}|r_{si}|r_{si}), \end{cases} \tag{6}$$

where (x_{si}, y_{si}) is defined as the position information of the i-th USV; ψ_{si} is defined as the yaw angle of the i-th USV; $\alpha_i = [\mu_{si}, v_{si}, r_{si}]^T$ are the surge, sway, and yaw velocity, respectively; $m_{\mu si}, m_{vsi}, m_{rsi}$ are the inertial mass; $f_{\mu si}(\alpha_i), f_{vsi}(\alpha_i), f_{rsi}(\alpha_i)$ are the nonlinear unknown functions consisting of the unmodeled hydrodynamics and Coriolis forces; and $\tau^f_{\mu si}$ and τ^f_{rsi} are the surge force and the yaw moment. $w_{\mu si}, w_{vsi}, w_{rsi}$ are the bounded disturbances caused by waves, wind, and ocean currents.

The hand position method is a control technique employed to manage the movement and positioning of USVs or similar underactuated systems. Underactuated systems have fewer control inputs than degrees of freedom, making traditional control strategies less effective. The hand position method addresses this challenge by defining a virtual control point (hand point) on the vehicle, allowing for more effective control. To deal with the underactuated USV motion model described by (4) and (5), the idea of the hand position method is considered. Define the front point (p_{six}, p_{siy}) of the USVs as the hand point, which can be formulated as

$$\begin{cases} p_{six} = x_{si} + L_{si}\cos\psi_{si}, \\ p_{siy} = y_{si} + L_{si}\sin\psi_{si}. \end{cases} \tag{7}$$

where L_{si} is the distance between the actual position (x_{si}, y_{si}) and the new defined hand point (p_{six}, p_{siy}), which is shown in Figure 1.

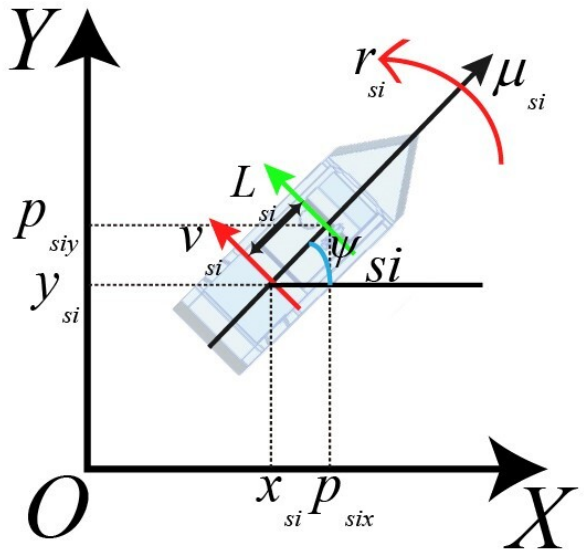

Figure 1. Motion model of USV.

Taking the second derivative of (7) shows that

$$\begin{cases} \ddot{p}_{six} = \dot{\mu}_{si}\cos\psi_{si} - (\dot{v}_{si} + L_{si}\dot{r}_{si})\sin\psi_{si} - \mu_{si}r_{si}\sin\psi_{si} - \left(v_{si}r_{si} + L_{si}r_{si}^2\right)\cos\psi_{si}, \\ \ddot{p}_{siy} = \dot{\mu}_{si}\sin\psi_{si} - (\dot{v}_{si} + L_{si}\dot{r}_{si})\cos\psi_{si} + \mu_{si}r_{si}\cos\psi_{si} - \left(v_{si}r_{si} + L_{si}r_{si}^2\right)\sin\psi_{si}, \end{cases} \tag{8}$$

substituting (6) into (8) yields that

$$\begin{cases} \ddot{p}_{six} = f_{six}(\beta) + \frac{\cos\psi_{si}}{m_{\mu si}}\tau_{\mu}^{f} - \frac{L_{si}\sin\psi_{si}}{m_{rsi}}\tau_{r}^{f} + w_{dix}, \\ \ddot{p}_{siy} = f_{siy}(\beta) + \frac{\sin\psi_{si}}{m_{\mu si}}\tau_{\mu}^{f} + \frac{L_{si}\cos\psi_{si}}{m_{rsi}}\tau_{r}^{f} + w_{diy}. \end{cases} \tag{9}$$

where

$$\begin{cases} f_{six}(\beta) = & f_{\mu}(\alpha)\cos\psi_{si} - (f_{v}(\alpha) + L_{si}f_{r}(\alpha))\sin\psi_{si} \\ & - \mu_{si}r_{si}\sin\psi_{si} - \left(v_{si}r_{si} + L_{si}r_{si}^{2}\right)\cos\psi_{si}, \\ f_{siy}(\beta) = & f_{\mu}(\alpha)\sin\psi_{si} + (f_{v}(\alpha) + L_{si}f_{r}(\alpha))\cos\psi_{si} \\ & + \mu_{si}r_{si}\cos\psi_{si} - \left(v_{si}r_{si} + L_{si}r_{si}^{2}\right)\sin\psi_{si}, \end{cases}$$

$$\begin{cases} w_{dix}(\beta) = \frac{w_{\mu si}}{m_{\mu si}}\cos\psi_{si} - \left(\frac{w_{vsi}}{m_{\mu si}} + \frac{L_{si}w_{rsi}}{m_{rsi}}\right)\sin\psi_{si}, \\ w_{diy}(\beta) = \frac{w_{\mu si}}{m_{\mu si}}\sin\psi_{si} + \left(\frac{w_{vsi}}{m_{\mu si}} + \frac{L_{si}w_{rsi}}{m_{rsi}}\right)\cos\psi_{si}, \end{cases}$$

with $\beta = [\mu_{si}, v_{si}, r_{si}, \psi_{si}]$.

Based on (9), the dynamics model of the i-th USV can be described as

$$\ddot{p}_{si} = f_{sixy} + \Omega_{si}(\psi_{si})\omega_{si}u_{si} + w_{dixy}. \tag{10}$$

where $p_{si} = \left[p_{six}, p_{siy}\right]^{T}$ is the position of the i-th ($i \in \Pi_2$) USV, and $f_{sixy} = \left[f_{six}, f_{siy}\right]^{T}$, $\Omega_{si}(\psi_{si}) = [\cos\psi_{si}, -\sin\psi_{si}; \sin\psi_{si}, \cos\psi_{si}]$, $u_{si} = \left[\tau_{\mu}, \tau_{r}\right]^{T}$, $\omega_{si} = \mathrm{diag}\{1/m_{\mu si}, L_{si}/m_{rsi}\}$, $w_{dixy} = \left[w_{dix}, w_{diy}\right]^{T}$.

To ensure the unity of the USV model and the UAV model, this formula is expanded and further converted to

$$\begin{bmatrix} \ddot{p}_{six} \\ \ddot{p}_{siy} \end{bmatrix} = \begin{bmatrix} f_{six} - \frac{L_{si}\sin\psi_{si}}{m_{rsi}}\tau_{ri} \\ f_{siy} + \frac{\sin\psi_{si}}{m_{\mu si}}\tau_{\mu i} \end{bmatrix} + \begin{bmatrix} \frac{\cos\psi_{si}}{m_{\mu si}} & 0 \\ 0 & \frac{L_{si}\cos\psi_{si}}{m_{rsi}} \end{bmatrix} \begin{bmatrix} \tau_{\mu i} \\ \tau_{ri} \end{bmatrix} + \begin{bmatrix} w_{dix} \\ w_{diy} \end{bmatrix}. \tag{11}$$

Combining (3) and (11), the unified model of the HMAS in the XY plane can be obtained:

$$\begin{cases} \dot{x}_{i1} = x_{i2} \\ \dot{x}_{i2} = F_{xi} + G_{xi}u_{xi} + \Delta_{xi}. \end{cases} \tag{12}$$

When Equation (12) represents the UAV model. Where $x_{i1} = x_{a1} \in \mathbb{R}^2$, $x_{i2} = x_{a2} \in \mathbb{R}^2$ is defined as the position and speed information of the UAV in the XY plane, $F_{xi} = f_{axy}$ is defined as unknown functions, $G_{xi} = g_{axy}$ is defined as coefficient matrix, $\Delta_{xi} = \Delta_{axy}$ indicates the external interference encountered by the UAV, $u_{xi} = u_{axy}$ is defined as coefficient matrix control input signal. When Equation (12) represents the USV model. where $x_{i1} = x_{si1} \in \mathbb{R}^2$, $x_{i2} = x_{si2} \in \mathbb{R}^2$ are the position and velocity of the i-th USV, $F_{xi} = F_{si} = \left[f_{six} - \frac{L_{si}\sin\psi_{si}}{m_{rsi}}\tau_{ri}, f_{siy} + \frac{\sin\psi_{si}}{m_{\mu si}}\tau_{\mu i} \right]^{T}$ is defined as unknown functions, $G_{xi} = G_{si}$ is defined as a coefficient matrix, $\Delta_{xi} = w_{dixy}$ is the bounded disturbances, $u_{xi} = u_{si}$ is defined as a coefficient matrix control input signal.

Similarly, consider the UAV model in the Z-axis direction as

$$\begin{cases} \dot{p}_{az} = v_{az}, \\ \dot{v}_{az} = f_{az} + \dfrac{1}{m_a} u_{az} + \Delta_{az} \\ \quad\;\; = F_{az} + G_{az} u_{az} + \Delta_{az}. \end{cases} \tag{13}$$

where p_{az} is the altitude of the UAV; v_{az} is defined as the speed of the UAV in the Z-axis, $F_{az} = -d_z \dot{p}_{az}/m_a - g$, and $G_{az} = \frac{1}{m_a}$.

The quantification technique can convert the initial continuous signal into a signal that is segmented and constant; the HMAS model with input quantization is represented as

$$\begin{bmatrix} \dot{U}_{si} \\ \dot{V}_{si} \end{bmatrix} = \begin{bmatrix} f_{six} - \frac{L_{si} \sin \psi_{si}}{m_{rsi}} Q(\tau_{ri}) \\ f_{siy} + \frac{\sin \psi_{si}}{m_{\mu si}} Q(\tau_{\mu i}) \end{bmatrix} + \begin{bmatrix} \frac{\cos \psi_{si}}{m_{\mu si}} & 0 \\ 0 & \frac{L_{si} \cos \psi_{si}}{m_{rsi}} \end{bmatrix} \begin{bmatrix} Q(\tau_{\mu i}) \\ Q(\tau_{ri}) \end{bmatrix} + \begin{bmatrix} w_{dix} \\ w_{diy} \end{bmatrix}. \tag{14}$$

In a similar way,

$$\begin{bmatrix} \dot{U}_a \\ \dot{V}_a \end{bmatrix} = \begin{bmatrix} -\frac{d_x \dot{p}_{ax}}{m_a} \\ -\frac{d_y \dot{p}_{ay}}{m_a} \end{bmatrix} + \begin{bmatrix} m_a^{-1} & 0 \\ 0 & m_a^{-1} \end{bmatrix} \begin{bmatrix} Q(u_{ax}) \\ Q(u_{ay}) \end{bmatrix} + \begin{bmatrix} \Delta_{ax} \\ \Delta_{ay} \end{bmatrix}. \tag{15}$$

Combining (14) and (15), the HMAS model with input quantization is represented as

$$\begin{cases} \dot{x}_{i1} = x_{i2}, \\ \dot{x}_{i2} = F_{xi} + G_{xi} Q(u_{xi}) + \Delta_{xi}. \end{cases} \tag{16}$$

Based on (16), the unified dynamic model of an HMAS in the XY plane can be obtained as

$$\begin{bmatrix} U_i \\ V_i \end{bmatrix} = F_i + G_i Q(\tau_i) + \Delta_i, \tag{17}$$

where $F_i = [F_{iU}, F_{iV}]^T$, $Q(\tau_i) = [Q(\tau_{iU}), Q(\tau_{iV})]^T$, $G_i = diag[G_{iU}, G_{iV}]$, $\Delta_i = [\Delta_{iU}, \Delta_{iV}]^T$, and $\tau_i = u_{xi}$.

The uniform quantization has the characteristic of easy realization; it can be expressed as follows:

$$Q(\tau_{iU}) = k_{iU} round(\frac{\tau_{iU}}{k_{iU}}),$$

$$Q(\tau_{iV}) = k_{iV} round(\frac{\tau_{iV}}{k_{iV}}),$$

where k_{iU} and k_{iV} denote the quantized indexes. The round function can return a value rounded to a specified number of decimal places. During the quantization process, quantization errors will be generated, and the control system's performance could be reduced. A continuous and differentiable time-varying reference trajectory is defined as

$$p_0(t) = [x_0(t), y_0(t)]^T \in \mathbb{R}^2, \tag{18}$$

$\mathcal{G} = \{\mathcal{V}, \mathcal{E}\}$ represents the USV and UAV communication topology diagram, Where $\mathcal{V} = \{n_0, n_1, \ldots, n_N\}$ is the set of all nodes combined, denoting N agents in formation; $\mathcal{E} = \{(i,j) \in \mathcal{V} \times \mathcal{V}\}$ is a set of all edges, and $\mathcal{A} = [a_{ij}] \in \mathbb{R}^{N \times N}$is the adjacency matrix, when $(n_i, n_j) \in \mathcal{E}$, $a_{ij} = 1$; if not, $a_{ij} = 0$.

Assumption 1. *The aerodynamic drag coefficients d_{ix}, d_{iy}, and d_{iz} are bounded and unknown. The quadrotor UAV experiences external perturbations Δ_x, Δ_y, Δ_z, which are confined within certain bounds, fulfilling the conditions $\|\Delta_{ax}\| \leq \bar{\Delta}_{ax}$, $\|\Delta_{ay}\| \leq \bar{\Delta}_{ay}$, $\|\Delta_{az}\| \leq \bar{\Delta}_{az}$. Here, $\bar{\Delta}_{ax}$, $\bar{\Delta}_{ay}$, and $\bar{\Delta}_{az}$ represent unknown positive constants. The USV experiences external disturbances $w_{\mu si}, w_{vsi}, w_{rsi}$, which are confined within certain limits, fulfilling the conditions $\|w_{\mu si}\| \leq \bar{w}_{\mu si}$, $\|w_{vsi}\| \leq \bar{w}_{vsi}$, $\|w_{rsi}\| \leq \bar{w}_{rsi}$. In this context, $\bar{w}_{\mu si}, \bar{w}_{vsi}$, and $\bar{w}_{rsi}$ signify unknown positive constants.*

Remark 1. *The complexity of operating environments introduces unpredictable aerodynamic forces, complicating the acquisition of precise system parameters. Moreover, considering that UAVs and USVs are not operated under extreme weather conditions, it renders Assumption 1 both justified and pragmatic.*

In this paper, a distributed controller is considered for each unmanned agent to ensure that each USV and UAV can track the expected time-varying trajectory and ensure

$$\lim_{t\to\infty} \|p_i(t) - p_{id}(t) - p_0(t)\| \leq l_{i0}, \tag{19}$$

where l_{i0} is a positive constant, and $p_{id}(t) \in \mathbb{R}^2$ is the position deviation relative to the parameterized path. $p_i(t) = [x_i(t), y_i(t)]^T \in \mathbb{R}^2$.

3. Controller Design

This section presents a formation control strategy that employs the ESO, designed to direct the HMAS to adhere to a specified trajectory within the XY plane. Following this, a decentralized formation control mechanism is formulated, focusing on the altitude tracking of the UAV in the Z-axis. The formation control flowchart of the HMAS is shown in Figure 2.

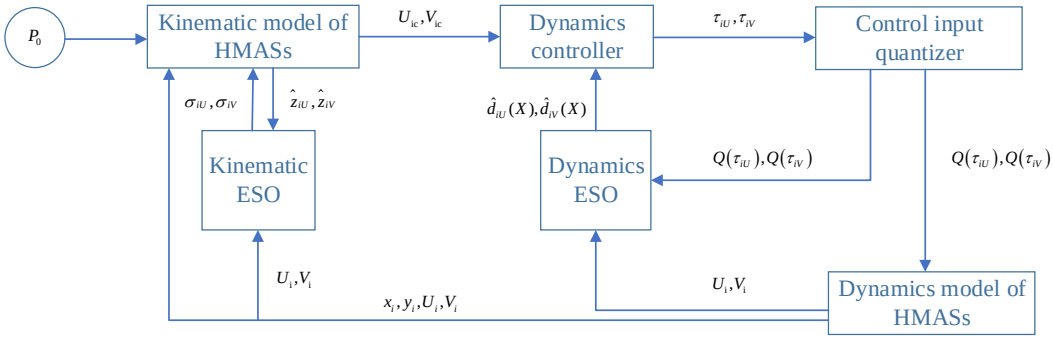

Figure 2. Formation control flowchart of HMAS.

3.1. Kinematic Controller Design

The formation error can be defined as

$$z_i = \sum_{j=1}^{N} a_{ij}(p_i - p_j - p_{ijd}) + a_{i0}(p_i - p_0 - p_{id}), \tag{20}$$

where $p_{ijd} = p_{id} - p_{jd} \in \mathbb{R}^2$ is the relative position deviation between HMAS .

Then, the time derivative of (20) can be obtained as follows:

$$\dot{z}_i = \sum_{j=1}^{N} a_{ij}\{[U_i, V_i]^T - [U_j, V_j]^T - \dot{p}_{ijd}\} + a_{i0}[U_i, V_i]^T - a_{i0}\dot{p}_0 - a_{i0}\dot{p}_{id}, \tag{21}$$

which can be rewritten as

$$\dot{z}_i = d_i[U_i, V_i]^T - a_{i0}\dot{p}_0 + \sigma_i, \tag{22}$$

where $d_i = \sum_{j=0}^{N} a_{ij}$, and σ_i is defined as $\sigma_i = -\sum_{j=1}^{N} a_{ij}[U_j, V_j]^T - \sum_{j=0}^{N} a_{ij} p_{ijd}$.

Assumption 2. *Since the velocity and acceleration of HMAS are both upper bounds, the unknown term σ_i is assumed to satisfy $\|\dot{\sigma}_i\| \leq \sigma^*$, where σ^* is a positive constant. The extended state observer can be used to observe the unknown term σ_i.*

The ESO is designed as follows:

$$\begin{cases} \dot{\hat{z}}_i = \vartheta_i + \hat{\sigma}_i - k_{i1}\tilde{z}_i, \\ \dot{\hat{\sigma}}_i = -k_{i2}\tilde{z}_i. \end{cases} \tag{23}$$

where $\tilde{z}_i = \hat{z}_i - z_i$ is defined as the ESO estimation error and $\vartheta_i = d_i[U_i, V_i]^T - a_{i0}\dot{p}_0$. Based on (22) and (23), it can be found that

$$\begin{cases} \dot{\tilde{z}}_i = \tilde{\sigma}_i - k_{i1}\tilde{z}_i, \\ \dot{\tilde{\sigma}}_i = -k_{i2}\tilde{z}_i - \dot{\sigma}_i. \end{cases} \tag{24}$$

Equation (24) can be rewritten as

$$\dot{\tilde{E}}_{i1} = A_i\tilde{E}_{i1} + B_i, \tag{25}$$

where $\tilde{E}_{i1} = [\tilde{z}_i, \tilde{\sigma}_i]^T$, and

$$A_i = \begin{bmatrix} -k_{i1} & 1 \\ -k_{i2} & 0 \end{bmatrix}, B_i = \begin{bmatrix} 0_2 \\ \dot{\sigma}_i \end{bmatrix}. \tag{26}$$

At the kinematic level, a distributed control law considering ESO is designed:

$$\begin{bmatrix} U_{ic} \\ V_{ic} \end{bmatrix} = d^{-1}[-\chi_i z_i + a_{i0}\dot{p}_0 - \hat{\sigma}_i], \tag{27}$$

where $\chi_i = diag[k_{ix}, k_{iy}] \in \mathbb{R}^2$ is positive constant.

3.2. Dynamic Controller Design

The control objective of the dynamic subsystem is

$$\begin{cases} \lim\limits_{t\to\infty} |e_{iU}| = |U_i - U_{id}| \leq \delta_1, \\ \lim\limits_{t\to\infty} |e_{iV}| = |V_i - V_{id}| \leq \delta_2, \end{cases} \tag{28}$$

where δ_1, δ_2 is positive constant, Let $Q(\tau_{iU}) = q_{1iU}(t)\tau_{iU} + q_{2iU}(t)$, $Q(\tau_{iV}) = q_{1iV}(t)\tau_{iV} + q_{2iV}(t)$, and

$$\begin{cases} q_{1iU}(t) = \begin{cases} \frac{Q(\tau_{iU}(t))}{\tau_{iU}(t)} & |\tau_{iU}(t)| \geq a \\ 1 & |\tau_{iU}(t)| < a \end{cases}, \\ q_{1iV}(t) = \begin{cases} \frac{Q(\tau_{iV}(t))}{\tau_{iV}(t)} & |\tau_{iV}(t)| \geq a \\ 1 & |\tau_{iV}(t)| < a \end{cases}, \\ q_{2iU}(t) = \begin{cases} 0 & |\tau_{iU}(t)| \geq a \\ Q(\tau_{iU}(t)) - \tau_{iU}(t) & |\tau_{iU}(t)| < a \end{cases}, \\ q_{2iV}(t) = \begin{cases} 0 & |\tau_{iV}(t)| \geq a \\ Q(\tau_{iV}(t)) - \tau_{iV}(t) & |\tau_{iV}(t)| < a \end{cases}, \end{cases} \tag{29}$$

where $q_{1iU}(t)$, $q_{1iV}(t)$ are unknown. Since the positive and negative values of the signal are not changed by the quantization process, $q_{1iU}(t)$, $q_{1iV}(t)$ are obtained. If $|\tau_{iU}(t)| < a$, $|\tau_{iV}(t)| < a$, then $Q(\tau_{iU}(t))$, $Q(\tau_{iV}(t))$ are bounded since $q_{2iU}(t)$, $q_{2iv}(t)$ are bounded. $|q_{2iU}(t)| \leq \bar{q}_2$, $|q_{2iV}(t)| \leq \bar{q}_2$.

Consider the following two sliding mode functions:

$$\begin{cases} s_{iU} = c_{iU} \int_0^t e_{iU} \mathrm{d}t + e_{iU}(t), \\ s_{iV} = c_{iV} \int_0^t e_{iV} \mathrm{d}t + e_{iV}(t), \end{cases} \tag{30}$$

where $s_i = [s_{iU}, s_{iV}]^T$, $c_{iU} > 0$ and $c_{iV} > 0$. The time derivative of (30) shows that

$$\dot{s}_{iU} = c_{iU} e_{iU} + \dot{e}_{iU} = G_{iU} q_{1iU}(t) \tau_{iU} + G_{iU} q_{2iU}(t) + \Delta_{iU} + F_{iU} - \dot{U}_{id} + c_{iU} e_{iU}. \tag{31}$$

$$\dot{s}_{iV} = c_{iV} e_{iV} + \dot{e}_{iV} = G_{iV} q_{1iV}(t) \tau_{iV} + G_{iV} q_{2iV}(t) + \Delta_{iV} + F_{iV} - \dot{V}_{id} + c_{iV} e_{iV}. \tag{32}$$

Let $d_{iU}(X) = \Delta_{iU} + F_{iU}, d_{iV}(X) = \Delta_{iV} + F_{iV}$, it follows that

$$\begin{aligned} s_{iU}\dot{s}_{iU} \leq s_{iU}[&-l_{iU}s_{iU} - \eta_{iU}\mathrm{sgn}s_{iU} + l_{iU}s_{iU} + \\ &\eta_{iU}\mathrm{sgn}s_{iU} + \tfrac{1}{2}G_{iU}s_{iU} + d_{iU}(X) + c_{iU}e_{iU} - \dot{U}_{id}\Big] \\ &+ s_{iU}G_{iU}q_{1iU}\tau_{iU} + \tfrac{1}{2}G_{iU}\bar{q}_{2iU}^2. \end{aligned} \tag{33}$$

$$\begin{aligned} s_{iV}\dot{s}_{iV} \leq s_{iV}[&-l_{iV}s_{iV} - \eta_{iV}\mathrm{sgn}s_{iV} + l_{iV}s_{iV} + \\ &\eta_{iV}\mathrm{sgn}s_{iV} + \tfrac{1}{2}G_{iV}s_{iV} + d_{iV}(X) + c_{iV}e_{iV} - \dot{V}_{id}\Big] \\ &+ s_{iV}G_{iV}q_{1iV}\tau_{iV} + \tfrac{1}{2}G_{iV}\bar{q}_{2iV}^2. \end{aligned} \tag{34}$$

where the 'sgn(x)' function is a mathematical function that extracts the sign of a real number. It is defined as follows: If the input x is negative, the output of 'sgn(x)' function is -1. If the input x is zero, the output of 'sgn(x)' function is 0. If the input x is positive, the output of 'sgn(x)' function is 1.

Since the specific function value of $d_i(X) = [d_{iU}, d_{iV}]^T$ is unknown, the extended state observer can be used to observe it:

$$\begin{cases} \dot{\tilde{p}}_i = G_i[Q(\tau_{iU}), Q(\tau_{iV})]^T + \hat{d}_i(X) - b_{i1}\tilde{p}_i, \\ \dot{\hat{d}}_i(X) = -b_{i2}\tilde{p}_i, \end{cases} \tag{35}$$

where $\tilde{p}_i = \hat{p}_i - p_i$ is the ESO estimation error; we have

$$\begin{cases} \ddot{\tilde{p}}_i = \dot{\tilde{d}}_i(X) - b_{i1}\dot{\tilde{p}}_i, \\ \dot{\tilde{d}}_i(X) = -b_{i2}\dot{\tilde{p}}_i - \dot{d}_i(X), \end{cases} \tag{36}$$

Which can be reshaped into

$$\dot{\tilde{E}}_{i2} = C_i \tilde{E}_{i2} + D_i, \tag{37}$$

where $\tilde{E}_{i2} = \left[\dot{\tilde{p}}_i, \tilde{d}_i(X)\right]^T$, and

$$C_i = \begin{bmatrix} -b_{i1} & 1 \\ -b_{i2} & 0 \end{bmatrix}, D_i = \begin{bmatrix} 0_2 \\ \dot{d}_i(X) \end{bmatrix}. \tag{38}$$

Define

$$\kappa_{iU} = l_{iU}s_{iU} + \eta_{iU}\mathrm{sgn}s_{iU} + \tfrac{1}{2}G_{iU}s_{iU} + \hat{d}_{iU}(X) + c_{iU}e_{iU} - \dot{U}_{id}, \tag{39}$$

where l_{iU} and η_{iU} are positive constants. It follows that

$$s_{iU}\dot{s}_{iU} \leq -l_{iU}s_{iU}^2 - \eta_{iU}|s_{iU}| + s_{iU}\kappa_{iU} + s_{iU}\tilde{d}_{iU}(X) + s_{iU}G_{iU}q_{1iU}\tau_{iU} + \frac{1}{2}G_{iU}\bar{q}_{2iU}^2, \tag{40}$$

where $\tilde{d}_{iU}(X) = d_{iU}(X) - \hat{d}_{iU}(X)$.

Similarly, let $\kappa_{iV} = l_{iV}s_{iV} + \eta_{iV}\,\mathrm{sgn}\,s_{iV} + \frac{1}{2}G_{iV}s_{iV} + \hat{d}_{iV}(X) + c_{iV}e_{iV} - \dot{V}_{id}$; it follows that

$$s_{iV}\dot{s}_{iV} \leq -l_{iV}s_{iV}^2 - \eta_{iV}|s_{iV}| + s_{iV}\kappa_{iV} + s_{iV}\tilde{d}_{iV}(X) + s_{iV}G_{iV}q_{1iV}\tau_{iV} + \frac{1}{2}G_{iV}\bar{q}_{2iV}^2. \tag{41}$$

Remark 2. *Because $q_{1iU}(t)$ and $q_{1iV}(t)$ are time-varying and unknown, adaptive estimation is adopted. The lower bounds of $q_{1iU}(t)$ and $q_{1iV}(t)$ are used for estimation to prevent singular problems that arise when the estimate is zero. Time-varying gains μ_{iU} and μ_{iV} are defined as $1/q_{1iU\min}$ and $1/q_{1iV\min}$, respectively, where $q_{1iU\min}$ and $q_{1iV\min}$ represent the lower bounds of $q_{1iU}(t)$ and $q_{1iV}(t)$.*

The dynamic controllers and adaptive laws are designed as follows:

$$\begin{cases} \tau_{iU} = -G_{iU}^{-1}\frac{s_{iU}\hat{\mu}_{iU}^2\kappa_{iU}^2}{|s_{iU}\hat{\mu}_{iU}\kappa_{iU}|+\rho_{iU}}, \\ \tau_{iV} = -G_{iV}^{-1}\frac{s_{iV}\hat{\mu}_{iV}^2\kappa_{iV}^2}{|s_{iV}\hat{\mu}_{iV}\kappa_{iV}|+\rho_{iV}}, \end{cases} \tag{42}$$

$$\begin{cases} \dot{\hat{\mu}}_{iU} = \gamma_1 s_{iU}\kappa_{iU} - \gamma_1\varsigma_{iU}\hat{\mu}_{iU}, \\ \dot{\hat{\mu}}_{iV} = \gamma_2 s_{iV}\kappa_{iV} - \gamma_2\varsigma_{iV}\hat{\mu}_{iV}, \end{cases} \tag{43}$$

where $\rho_{iU}, \rho_{iV}, \gamma_1, \gamma_2, \varsigma_{iU}, \varsigma_{iV}$ are positive constants.

The error subsystem generated by z_i, s_{iU}, s_{iV}, $\tilde{\mu}_{iU}$, $\tilde{\mu}_{iV}$ is as follows:

$$\begin{cases} \dot{z}_i = -\chi_i z_i - \tilde{\sigma}_i, \\ \dot{s}_{iU} = c_{iU}e_{iU} + \dot{e}_{iU}, \\ \dot{s}_{iV} = c_{iV}e_{iV} + \dot{e}_{iV}, \\ \dot{\tilde{\mu}}_{iU} = \dot{\hat{\mu}}_{iU} - \dot{\mu}_{iU} = \gamma_1 s_{iU}\kappa_{iU} - \gamma_1\varsigma_{iU}\hat{\mu}_{iU}, \\ \dot{\tilde{\mu}}_{iV} = \dot{\hat{\mu}}_{iV} - \dot{\mu}_{iV} = \gamma_2 s_{iV}\kappa_{iV} - \gamma_2\varsigma_{iV}\hat{\mu}_{iV}. \end{cases} \tag{44}$$

3.3. Altitude Controller Design of UAV

The height error system is defined as

$$\begin{cases} e_{azp} = p_{az} - p_{azd}, \\ e_{azv} = v_{az} - v_{azd}, \end{cases} \tag{45}$$

where p_{azd} is defined as the desired position information, and v_{azd} is defined as the desired velocity information.

Consider the following input and adaptive laws:

$$\begin{cases} u_{az} = \hat{G}_{az}^{-1}\left(-\sigma_z e_\zeta - \frac{e_\zeta\hat{\kappa}_{11}h^Th}{2\varsigma_1^2} - \frac{e_\zeta\hat{\kappa}_{12}}{2\varsigma_2^2} + \dot{v}_{azd} - k_\zeta e_{azv}\right), \\ \dot{\hat{\kappa}}_{11} = l_{11}\left(-k_{11}\hat{\kappa}_{11} + \frac{e_\zeta^Te_\zeta h^Th}{2\varsigma_1^2}\right), \\ \dot{\hat{\kappa}}_{12} = l_{12}\left(-k_{12}\hat{\kappa}_{12} + \frac{e_\zeta^Te_\zeta}{2\varsigma_2^2}\right), \\ \dot{\hat{G}}_{az} = \mathrm{Pr}\,oj_{\left[\hat{G}_{az},\bar{G}_{az}\right]}\{S\} = \begin{cases} 0 & \text{if } \hat{G}_{az} = \bar{G}_{az}, S \geq 0 \\ & \text{or } \hat{G}_{az} = \widehat{G}_{az}, S \leq 0, \\ S & \text{otherwise,} \end{cases} \end{cases} \tag{46}$$

where $S = \iota_{13}(-k_{13}\hat{G}_{az} + e_\zeta u_{az})$, and $\bar{G}_{az}$, $\widehat{G}_{az}$ is the lower and maximum bound of $\hat{G}_{az}$. $k_{11}, k_{12}, k_{13}, \sigma_z, \iota_{11}, \iota_{12}, \iota_{13}, k_\zeta, \varsigma_1, \varsigma_2$ are positive parameters to be designed.

Remark 3. *An adaptive law (43) is used to estimate quantization parameters to ensure that the designed dynamic control law (42) does not depend on quantization information. Quantization parameters can be adjusted according to the needs of system performance.*

4. Stability Analysis

Theorem 1. *System (25) consists of the said input $\dot{\sigma}_i$ and states $\tilde{z}_i$, $\tilde{\sigma}_i$. The system is input-state stable, so that for every bounded input over an infinite time horizon, the state of the system also remains bounded.*

Proof. The following Lyapunov function is designed:

$$\dot{V}_1 = \sum_{i=1}^{N} \tilde{E}_{i1}^T P_i \tilde{E}_{i1}, \tag{47}$$

where P_i represents a positive definite matrix which complies with $A_i^T P_i + P_i^T A_i \leq I$.

Then, the time derivative of (25) can be obtained as follows:

$$\dot{V}_1 \leq \sum_{i=1}^{N} \{-E_{i1}^T E_{i1} + E_{i1}^T P_i B_i \dot{\sigma}_i\}. \tag{48}$$

Due to

$$\|E_{i1}\| \geq \frac{\|P_i B_i\| \|\dot{\sigma}_i\|}{\bar{\theta}_{i1}}, \tag{49}$$

we obtain

$$\dot{V}_1 \leq -\sum_{i=1}^{N} (1 - \bar{\theta}_{i1}) \|E_{i1}\|^2, \tag{50}$$

where $0 < \bar{\theta}_{i1} < 1$. For input $\dot{\sigma}_i$, the subsystem (25) is stable from input to state, and

$$\|E_{i1}(t)\| \leq \sqrt{\frac{\lambda_{\max}(P_i)}{\lambda_{\min}(P_i)}} \max\left\{ \|E_{i1}(t_0)\| e^{-\varrho_{i1}(t-t_0)}, \frac{\|P_i B_i\| \sigma^*}{\bar{\theta}_{i1}} \right\}, \quad \forall t \geq t_0, \tag{51}$$

where $\varrho_{i1} = \left(1 - \bar{\theta}_{i1}\right) / \lambda_{\max}(P_i)$. □

Theorem 2. *System (37) consists of the said input $\dot{d}_i(X)$ and states $\tilde{p}_i$, $\tilde{d}_i(X)$. The system is input-state stable so that for every bounded input over an infinite time horizon, the state of the system also remains bounded.*

Proof. The following Lyapunov function is designed:

$$\dot{V}_2 = \sum_{i=1}^{N} \tilde{E}_{i2}^T Q_i \tilde{E}_{i2}, \tag{52}$$

where Q_i represents a positive definite matrix which complies with

$$C_i^T Q_i + Q_i^T C_i \leq I. \tag{53}$$

Then, the time derivative of (37) can be obtained as follows:

$$\dot{V}_2 \leq \sum_{i=1}^{N} \left\{ -E_{i2}^T E_{i2} + E_{i2}^T Q_i D_i \dot{d}_i(X) \right\}, \tag{54}$$

since

$$\|E_{i2}\| \geq \frac{\|Q_i D_i\| \left\|\dot{d}_i(X)\right\|}{\bar{\theta}_{i2}}, \tag{55}$$

we obtain $\dot{V}_2 \leq -\sum_{i=1}^{N}(1-\bar{\theta}_{i2})\|E_{i2}\|^2$, where $0 < \bar{\theta}_{i2} < 1$. For input $\dot{d}_i(X)$, the subsystem (37) is stable from input to state, and

$$\|E_{i2}(t)\| \leq \sqrt{\frac{\lambda_{\max}(Q_i)}{\lambda_{\min}(Q_i)}} \max\left\{\|E_{i2}(t_0)\|e^{-\varrho_{i2}(t-t_0)}, \frac{\|Q_i D_i\| d(X)^*}{\bar{\theta}_{i2}}\right\}, \quad \forall t \geq t_0, \tag{56}$$

where $\varrho_{i2} = \left(1-\bar{\theta}_{i2}\right)/\lambda_{\max}(Q_i)$. □

Theorem 3. *The dynamic error subsystem (44), viewed as the system with the states being $z_i, s_{iU}, s_{iV}, \tilde{\mu}_{iU}, \tilde{\mu}_{iV}$ and the inputs being $q_{2iU}, q_{2iV}, \mu_{iU}, \mu_{iV}, \tilde{\sigma}_i$, is stable from input to state.*

Proof. Define the following Lyapunov function:

$$V_3 = \sum_{i=1}^{N}\left\{\frac{1}{2}s_{iU}^2 + \frac{1}{2\gamma_1\mu_{iU}}\tilde{\mu}_{iU}^2 + \frac{1}{2}s_{iV}^2 + \frac{1}{2\gamma_2\mu_{iV}}\tilde{\mu}_{iV}^2 + \frac{1}{2}z_i^T z_i\right\} \tag{57}$$

where $\mu_{iU} > 0$ and $\mu_{iV} > 0$.

Then, the time derivative of (57) can be obtained as follows:

$$\dot{V}_3 = \sum_{i=1}^{N}\left\{s_{iU}\dot{s}_{iU} + \frac{1}{\gamma_1\mu_{iU}}\tilde{\mu}_{iU}\dot{\hat{\mu}}_{iU} + s_{iV}\dot{s}_{iV} + \frac{1}{\gamma_2\mu_{iV}}\tilde{\mu}_{iV}\dot{\hat{\mu}}_{iV} + z_i^T\dot{z}_i\right\}. \tag{58}$$

Substituting Equations (40)–(43) into (58), it can be seen that

$$\begin{aligned}\dot{V}_3 \leq \sum_{i=1}^{N}\Bigg\{&-\left(l_{iU}-\frac{1}{2}\right)s_{iU}^2 - \eta_{iU}|s_{iU}| + s_{iU}\kappa_{iU} + \frac{1}{2}G_{iU}\bar{q}_{2iU}^2\\ &- q_{1iU}\frac{s_{iU}^2\hat{\mu}_{iU}^2\kappa_{iU}^2}{|s_{iU}\hat{\mu}_{iU}\kappa_{iU}| + \rho_{iU}} + \frac{1}{\gamma_1\mu_{iU}}\tilde{\mu}_{iU}(\gamma_1 s_{iU}\kappa_{iU} - \gamma_1\varsigma_{iU}\hat{\mu}_{iU})\\ &-\left(l_{iV}-\frac{1}{2}\right)s_{iV}^2 - \eta_{iV}|s_{iV}| + s_{iV}\kappa_{iV} + \frac{1}{2}G_{iV}\bar{q}_{2iV}^2 - q_{1iV}\frac{s_{iV}^2\hat{\mu}_{iV}^2\kappa_{iV}^2}{|s_{iV}\hat{\mu}_{iV}\kappa_{iV}| + \rho_{iV}}\\ &+\frac{1}{\gamma_2\mu_{iV}}\tilde{\mu}_{iV}(\gamma_2 s_{iV}\kappa_{iV} - \gamma_2\varsigma_{iV}\hat{\mu}_{iV}) + z_i^T\dot{z}_i + \frac{1}{2}\tilde{d}_{iU}^2(X) + \frac{1}{2}\tilde{d}_{iV}^2(X).\Bigg\}\end{aligned} \tag{59}$$

From $|a| - \frac{a^2}{\rho+|a|} < \rho$ and considering $q_{1iU} \geq q_{1iU\min} = 1/\mu_{iU} > 0$ and $q_{1iV} \geq q_{1iV\min} = 1/\mu_{iV} > 0$, we have

$$\begin{aligned}\dot{V}_3 \leq \sum_{i=1}^{N}\Bigg\{&-\left(l_{iU}-\frac{1}{2}\right)s_{iU}^2 - \eta_{iU}|s_{iU}| + \frac{1}{2}G_{iU}\bar{q}_{2iU}^2 + \frac{1}{\mu_{iU}}\rho_{iU} - \frac{1}{\mu_{iU}}\tilde{\mu}_{iU}\varsigma_{iU}\hat{\mu}_{iU} - \left(l_{iV}-\frac{1}{2}\right)s_{iV}^2\\ &-\eta_{iV}|s_{iV}| + \frac{1}{2}G_{iV}\bar{q}_{2iV}^2 + \frac{1}{\mu_{iV}}\rho_{iV} - \frac{1}{\mu_{iV}}\tilde{\mu}_{iV}\varsigma_{iV}\hat{\mu}_{iV} + z_i^T\dot{z}_i + \frac{1}{2}\tilde{d}_{iU}^2(X) + \frac{1}{2}\tilde{d}_{iV}^2(X)\Bigg\}.\end{aligned} \tag{60}$$

Noting that

$$\begin{cases} -\tilde{\mu}_{iU}\hat{\mu}_{iU} \leq -\frac{1}{2}\tilde{\mu}_{iU}^2 + \frac{1}{2}\mu_{iU}^2,\\ -\tilde{\mu}_{iV}\hat{\mu}_{iV} \leq -\frac{1}{2}\tilde{\mu}_{iV}^2 + \frac{1}{2}\mu_{iV}^2, \end{cases} \tag{61}$$

it follows that (60) can be put into

$$\begin{aligned}\dot{V}_3 \le \sum_{i=1}^{N}\Bigg\{ &-\left(l_{iU}-\frac{1}{2}\right)s_{iU}^2-\eta_{iU}|s_{iU}|+\frac{1}{2}G_{iU}\bar{q}_{2iU}^2\\ &+\frac{1}{\mu_{iU}}\rho_{iU}-\frac{1}{2\mu_{iU}}\varsigma_{iU}\tilde{\mu}_{iU}^2+\frac{1}{2}\varsigma_{iU}\mu_{iU}-\left(l_{iV}-\frac{1}{2}\right)s_{iV}^2-\eta_{iV}|s_{iV}|+\frac{1}{2}G_{iV}\bar{q}_{2iV}^2\\ &+\frac{1}{\mu_{iV}}\rho_{iV}-\frac{1}{2\mu_{iV}}\varsigma_{iV}\tilde{\mu}_{iV}^2+\frac{1}{2}\varsigma_{iV}\mu_{iV}+z_i^T\dot{z}_i+\frac{1}{2}\bar{d}_{iU}^2(X)+\frac{1}{2}\bar{d}_{iV}^2(X)\Bigg\}.\end{aligned} \tag{62}$$

where $D_{iU}=G_{iU}\bar{q}_{2iU}^2/2+\rho_{iU}/\mu_{iU}+\varsigma_{iU}\mu_{iU}/2$, $D_{iV}=G_{iV}\bar{q}_{2iV}^2/2+\rho_{iV}/\mu_{iV}+\varsigma_{iV}\mu_{iV}/2$.

Equation (62) can be reshaped into

$$\begin{aligned}\dot{V}_3 \le \sum_{i=1}^{N}\Bigg\{ &-\left(l_{iU}-\frac{1}{2}\right)s_{iU}^2-\eta_{iU}|s_{iU}|-\frac{1}{2\mu_{iU}}\varsigma_{iU}\tilde{\mu}_{iU}^2\\ &+D_{iU}-\left(l_{iV}-\frac{1}{2}\right)s_{iV}^2-\eta_{iV}|s_{iV}|-\frac{1}{2\mu_{iV}}\varsigma_{iV}\tilde{\mu}_{iV}^2\\ &+D_{iV}+z_i^T\dot{z}_i+\frac{1}{2}\bar{d}_{iU}^2(X)+\frac{1}{2}\bar{d}_{iV}^2(X)\Bigg\}.\end{aligned} \tag{63}$$

Substituting (44) into (63), it can be seen that

$$\begin{aligned}\dot{V}_3 \le \sum_{i=1}^{N}\Bigg\{ &-\left(l_{iU}-\frac{1}{2}\right)s_{iU}^2-\left(l_{iV}-\frac{1}{2}\right)s_{iV}^2\\ &-\frac{1}{2\mu_{iU}}\varsigma_{iU}\tilde{\mu}_{iU}^2-\frac{1}{2\mu_{iV}}\varsigma_{iV}\tilde{\mu}_{iV}^2-z_i^T\chi_i z_i\\ &+D_{iU}+D_{iV}-z_i^T\tilde{\sigma}_i+\frac{1}{2}\bar{d}_{iU}^2(X)+\frac{1}{2}\bar{d}_{iV}^2(X)\Bigg\},\end{aligned} \tag{64}$$

it follows that

$$\begin{aligned}\dot{V}_3 \le \sum_{i=1}^{N}\Bigg\{ &-\left(l_{iU}-\frac{1}{2}\right)s_{iU}^2-\left(l_{iV}-\frac{1}{2}\right)s_{iV}^2\\ &-\frac{1}{2\mu_{iU}}\varsigma_{iU}\tilde{\mu}_{iU}^2-\frac{1}{2\mu_{iV}}\varsigma_{iV}\tilde{\mu}_{iV}^2-\left(\lambda_{\min}(\chi_i)-\frac{1}{2}\right)\|z_i\|^2\\ &+D_{iU}+D_{iV}+\frac{1}{2}\|\tilde{\sigma}_i\|^2+\frac{1}{2}\bar{d}_{iU}^2(X)+\frac{1}{2}\bar{d}_{iV}^2(X)\Bigg\}.\end{aligned} \tag{65}$$

where $z=[z_1^T,z_2^T,\ldots,z_N^T]^T$, $s_U=[s_{1U},s_{2U},\ldots,s_{NU}]^T$, $s_V=[s_{1V},s_{2V},\ldots,s_{NV}]^T$, $\tilde{\mu}_U=[\tilde{\mu}_{1U},\tilde{\mu}_{2U},\ldots,\tilde{\mu}_{NU}]^T$, $\tilde{\mu}_V=[\tilde{\mu}_{1V},\tilde{\mu}_{2V},\ldots,\tilde{\mu}_{NV}]^T$, $\hbar_3=\min_{i=1,\ldots,N}[l_{iU}-\frac{1}{2},l_{iV}-\frac{1}{2},\varsigma_{iU}/2\mu_{iU},\varsigma_{iV}/2\mu_{iV},\lambda_{\min}(\chi_i)-\frac{1}{2}]$, $E_3=[s_U,s_V,\tilde{\mu}_U,\tilde{\mu}_V,z]$.

This indicates that

$$\dot{V}_3 \le -(1-\bar{\theta}_3)\hbar_3\|E_3\|^2-\bar{\theta}_3\hbar_3\|E_3\|^2+\sum_{i=1}^{N}(D_{iU}+D_{iV}+\tfrac{1}{2}\|E_{i1}\|^2+\tfrac{1}{2}\|E_{i2}\|^2), \tag{66}$$

noting that

$$\|E_3\| \ge \sum_{i=1}^{N}\left(\sqrt{\frac{2D_{iU}+2D_{iV}+\|E_{i1}\|^2+\|E_{i2}\|^2}{2\bar{\theta}_3\hbar_3}}\right), \tag{67}$$

renders

$$\dot{V}_3 \le -(1-\bar{\theta}_3)\hbar_3\|E_3\|^2, \tag{68}$$

where $0 < \bar{\theta}_2 < 1$; it is concluded that the subsystem (44) is input-state stable, and

$$\begin{aligned} \|E_3(t)\| \leq \sqrt{\frac{\lambda_{\max}(P_c)}{\lambda_{\min}(P_c)}} \max\Big\{ \|E_3(t_0)\| e^{-\varrho_3(t-t_0)} \\ \sum_{i=1}^{N} \left(\sqrt{\frac{2D_{iU} + 2D_{iV} + \|E_{i1}\|^2 + \|E_{i2}\|^2}{2\bar{\theta}_3 \hbar_3}} \right) \Big\}, \quad \forall t \geq t_0, \end{aligned} \tag{69}$$

where $\varrho_3 = 2\hbar_3(1-\bar{\theta}_3)/\lambda_{\max}(P_c)$ and $P_c = \mathrm{diag}\Big\{1, \frac{1}{2}\gamma_1\mu_{1U}, \ldots, \frac{1}{2}\gamma_1\mu_{NU}, \frac{1}{2}\gamma_2\mu_{1V}, \ \ldots, \frac{1}{2}\gamma_2\mu_{NV}\Big\}$.

The stability of the closed-loop control system is analyzed as follows. □

Theorem 4. *Consider (16), (27), (42) and (43), the cascade system is input-state stable, and all signals are uniformly ultimately bounded.*

Proof. Considering the stability theorem for cascaded systems proposed by Sontag and Wang in [44] and combining Theorems 1 and 2, it follows that the closed-loop system which is composed of (25) and (44) is input-state stable. From (51) and (69), $\|E_3(t)\|$ is eventually bounded by

$$\|E_3(t)\| \leq \sqrt{\frac{\lambda_{\max}(P_c)}{\lambda_{\min}(P_c)}} \sum_{i=1}^{N} \left\{ \sqrt{\frac{2D_{iU} + 2D_{iV} + \|E_{i2}\|^2}{2\bar{\theta}_3\hbar_3}} + \sqrt{\frac{\|P_i B_i\|^2 \sigma^{*2}}{2\bar{\theta}_3\hbar_3\bar{\theta}_{i1}^2}} \right\}. \tag{70}$$

This proof is complete. □

Theorem 5. *Suppose Assumptions 1 and 2 are valid and the condition $v_{azd} - \dot{p}_{azd} = 0$ is met. Under these circumstances, if the control scheme for formation tracking along with the adaptive law is implemented as outlined in (46), it leads to the UAV successfully tracking the desired height signal. Additionally, the tracking error eazp is ensured to be uniformly ultimately bounded.*

Proof. The time derivative of (45) can be obtained as follows:

$$\begin{cases} \dot{e}_{azp} = e_{azv}, \\ \dot{e}_{azv} = F_{az} + G_{az}u_{az} + \Delta_{az} - \dot{v}_{azd}. \end{cases} \tag{71}$$

In system (71), regarding e_{azv} as the virtual control input. Design the virtual control signal $\zeta_z = -k_\zeta e_{azp}$ to ensure the stability of system (71).

Design the following Lyapunov function:

$$V_{azp} = \frac{1}{2} e_{azp}^T e_{azp}, \tag{72}$$

then, the time derivative of (72) can be obtained as follows:

$$\dot{V}_{azp} = -k_\zeta e_{azp}^T e_{azp}. \tag{73}$$

Define a new error as

$$e_\zeta = e_{azv} - \zeta_z, \tag{74}$$

taking the time derivative of (74) and substituting (46) into it, it follows that

$$\begin{aligned}\dot{e}_\zeta =& -\sigma_\zeta e_\zeta + F_{az} + \Delta_{az} + \tilde{G}_{az}u_{az} - \\ & \frac{e_\zeta \hat{\kappa}_{11} h(X)^T h(X)}{2\varsigma_1^2} - \frac{e_\zeta \hat{\kappa}_{12}}{2\varsigma_2^2}.\end{aligned} \tag{75}$$

Define the following Lyapunov function:

$$V_z = \frac{1}{2}e_{azp}^T e_{azp} + \frac{1}{2}e_\zeta^T e_\zeta + \frac{\tilde{\kappa}_{i11}^2}{2\iota_{11}} + \frac{\tilde{\kappa}_{i12}^2}{2l_{12}} + \frac{\mathrm{Tr}\left(\tilde{G}_{az}^T \tilde{G}_{az}\right)}{2l_{13}}. \tag{76}$$

where $\tilde{\kappa}_{11} = \kappa_{11} - \hat{\kappa}_{11}, \tilde{\kappa}_{12} = \kappa_{12} - \hat{\kappa}_{12}$, and $\tilde{G}_{az} = G_{az} - \hat{G}_{az}$. The time derivative of (76) can be obtained as follows:

$$\begin{aligned}\dot{V}_z \le & -k_\zeta e_{azp}^T e_{azp} - \sigma_z e_\zeta^T e_\zeta + e_\zeta^T F_{az} + e_\zeta^T \Delta_{az} \\ & + e_\zeta^T \tilde{G}_{az} u_{az} - \frac{e_\zeta^T e_\zeta \hat{\kappa}_{11} h(X)^T h(X)}{2\varsigma_{i1}^2} - \frac{e_\zeta^T e_\zeta \hat{\kappa}_{12}}{2\varsigma_{i2}^2} + \frac{\tilde{\kappa}_{11}\dot{\tilde{\kappa}}_{11}}{\iota_{11}} + \frac{\tilde{\kappa}_{12}\dot{\tilde{\kappa}}_{12}}{\iota_{12}} + \frac{\mathrm{Tr}\left(\tilde{G}_{az}^T \dot{\tilde{G}}_{az}\right)}{l_{13}}.\end{aligned} \tag{77}$$

Since F_{az} is an unknown term, the RBFNN system is used to approximate it, $F_{az} = W_a^* h(X) + \varepsilon_a$, where W_a^* represents the ideal weight, ε_a represents the estimation error, $\|\varepsilon_a\| \le \bar{\varepsilon}_a$, and $h(X)$ denotes Gaussian functions.

Noting that

$$\begin{aligned}e_\zeta^T W_a^* h(X) &\le \frac{e_\zeta^T e_\zeta \kappa_{11} h(X)^T h(X)}{2\varsigma_{i1}^2} + \frac{\varsigma_{i1}^2}{2}, \\ e_\zeta^T (\varepsilon_a + \Delta_{az}) &\le \frac{e_\zeta^T e_\zeta \kappa_{i12}}{2\varsigma_{i2}^2} + \frac{\varsigma_{i2}^2}{2},\end{aligned} \tag{78}$$

where $\kappa_{11} = W_a^{*T} W_a^*$ and $\kappa_{12} = (\bar{\varepsilon}_a + \bar{\Delta}_{az})^T (\bar{\varepsilon}_a + \bar{\Delta}_{az})$.

Substituting (78) into (77), it follows that

$$\begin{aligned}\dot{V}_z \le & -k_\zeta e_{azp}^T e_{axp} - \sigma_z e_\zeta^T e_\zeta + \frac{e_\zeta^T e_\zeta \kappa_{11} h(X)^T h(X)}{2\varsigma_1^2} + \frac{e_\zeta^T e_\zeta \kappa_{12}}{2\varsigma_2^2} - \frac{e_\zeta^T e_\zeta \hat{\kappa}_{11} h^T(X) h(X)}{2\varsigma_1^2} \\ & - \frac{e_\zeta^T e_\zeta \hat{\kappa}_{i2}}{2\varsigma_2^2} - \tilde{\kappa}_{12}\left(-k_{12}\hat{\kappa}_{12} + \frac{e_\zeta^T e_\zeta}{2\varsigma_2^2}\right) - \tilde{\kappa}_{11}\left(-k_{11}\hat{\kappa}_{11} + \frac{e_\zeta^T e_\zeta h^T(X) h(X)}{2\varsigma_1^2}\right) + e_\zeta^T \tilde{G}_{az} u_{az} \\ & - \mathrm{Tr}\left(\tilde{G}_{az}^T\left(-k_{13}\hat{G}_{az} + e_\zeta u_{az}\right)\right) + \frac{\varsigma_1^2}{2} + \frac{\varsigma_2^2}{2} \\ \le & -k_\zeta e_{azp}^T e_{azp} - \sigma_z e_\zeta^T e_\zeta - \frac{k_{11}}{2}\tilde{\kappa}_{11}^2 - \frac{k_{12}}{2}\tilde{\kappa}_{12}^2 - \frac{k_{13}}{2}\left\|\tilde{G}_{az}\right\|_F^2 \\ & + \frac{k_{11}}{2}\kappa_{11}^2 + \frac{k_{12}}{2}\kappa_{12}^2 + \frac{k_{13}}{2}\|G_{az}\|_F^2 + \frac{\varsigma_1^2}{2} + \frac{\varsigma_2^2}{2} \\ \le & -\vartheta_z V_z + v_z.\end{aligned} \tag{79}$$

where $\vartheta_z = \min\left\{2k_\zeta, 2\sigma_z, \iota_{11}k_{11}, \iota_{12}k_{12}, \iota_{13}k_{13}\right\} > 0$, $v_z = \frac{k_{11}}{2}\kappa_{11}^2 + \frac{k_{12}}{2}\kappa_{12}^2 + \frac{k_{13}}{2}\|G_{az}\|_F^2 + \frac{\varsigma_1^2}{2} + \frac{\varsigma_2^2}{2}$.

According to (79), we can obtain

$$\dot{V}_z \le -\vartheta_z V_z + v_z. \tag{80}$$

The altitude tracking errors and velocity errors of the UAV are uniformly ultimately bounded. □

5. Illustrative Examples

In this section, we demonstrate the effectiveness of the controller presented in this paper by constructing a formation system comprising one UAV and four USVs, as outlined below. The model parameters of the HMAS are given in Table 1.

If $B = diag\{0, 0, 0, 0, 1\}$ is the adjacency weight matrix between agents and the virtual leader, then the adjacency matrix A and the Laplacian matrix L are as follows:

$$A = \begin{bmatrix} 0 & 1 & 1 & 0 & 1 \\ 1 & 0 & 1 & 1 & 0 \\ 1 & 1 & 0 & 0 & 0 \\ 0 & 1 & 0 & 0 & 0 \\ 1 & 0 & 0 & 0 & 0 \end{bmatrix} \quad L = \begin{bmatrix} 3 & -1 & -1 & 0 & -1 \\ -1 & 3 & -1 & -1 & 0 \\ -1 & -1 & 2 & 0 & 0 \\ 0 & -1 & 0 & 1 & 0 \\ -1 & 0 & 0 & 0 & 1 \end{bmatrix}$$

Table 1. Model Parameters.

Parameter	Value
m_a	2
g_a	9.8
J_{ax}, J_{ay}, J_{az}	1.5
d_{ax}, d_{ay}, d_{az}	0.012
$m_{\mu si}$	25.8
m_{vsi}	33.8
m_{rsi}	2.76
$d_{\mu si}$	0.725
d_{vsi}	0.89
d_{rsi}	−1.9
$d_{\mu bi1}$	−1.33
d_{vbi1}	−36.47
d_{rbi1}	−0.75
d_{rbi}	−1.9
f_{iv}	$-36.5\|v\|v - 0.8896v - 0.805v\|r\| - m_{i\mu}\mu r$
f_{ir}	$-0.75\|r\|r - 1.90r + 0.08\|v\|r$
	$+(m_{iu} - m_{iv})\mu v - 1.0948\mu r$

Case 1. Let leader UAV navigate along the time-varying parametric trajectory $p_0 = [1.2t, 0.2t]^T$. The initial states of five HMAS are set as $p_1 = [0, 0, 0]^T$, $p_2 = [-7, 7, 0]^T$, $p_3 = [-7, -7, 8]^T$, $p_4 = [-14, 14, 0]^T$, $p_5 = [-14, -14, 0]^T$. In the XY plane, the desired formation pattern is defined as $p_{1d} = [0, 0]^T$, $p_{2d} = [-7, 7]^T$, $p_{3d} = [-7, -7]^T$, $p_{4d} = [-14, 14]^T$, $p_{5d} = [-14, -14]^T$.

According to Equations (30), (39), (40), (42) and (43), the controller parameters are selected sequentially as $c_{iU} = c_{iV} = 10$, $l_{iU} = l_{iV} = 30$, $\eta_{iU} = \eta_{iV} = 2$, $\rho_{iU} = \rho_{iV} = 0.02$, $\varsigma_{iU} = \varsigma_{iV} = 0.2$, $\gamma_1 = \gamma_2 = 2$, $k_{iU} = k_{iV} = 0.2$. The external disturbances are given as $\Delta_{axz} = 0.3\cos(0.2t)$, $\Delta_{axy} = [0.2\cos(0.5t), 0.8\cos(t)]^T$, $\omega_{dixy} = [1.1\cos(0.5t), -0.2\sin(2t)]^T$, $p_{az} = 8$. The total duration of the simulation run is $T_z = 400$ s.

Figures 3–11 show the simulation results for the underactuated HMAS by using the proposed controller with input quantization. The trajectories of the HMAS in the 3D environment are depicted in Figure 3. It is clear from the figure that the HMAS set off from a given initial position, maintain the desired distance from each other, and maintain a special formation under the influence of external interference and system internal error. Figures 4 and 5 depict the longitudinal and lateral velocity of four USVs and one UAV in the XY plane. As can be seen from the figure, the speed synchronization between the USV and the UAV is achieved in around 30s. Figures 6 and 7 describe the formation tracking errors of four USVs and one UAV in the XY plane in both the lateral and longitudinal directions. It is clear that the HMAS can accomplish the formation mission under a small error. Figure 8 describes the longitudinal control input τ_{iU} and $Q(\tau_{iU})$ with and without

input quantization. Figure 9 describes the lateral control input τ_{iV} and $Q(\tau_{iV})$ with and without input quantization, respectively. Under comparison, the quantization process is able to guarantee the control signal can maintain the quality of the control scheme without losing control performance. The sliding mode function of USVs and UAV is depicted in Figure 11. The performance of ESO in estimating $d_i(X)$ is depicted in Figure 11, which clearly demonstrates the effectiveness of the proposed solution for the accurate compensation of uncertainties and external disturbances within heterogeneous systems.

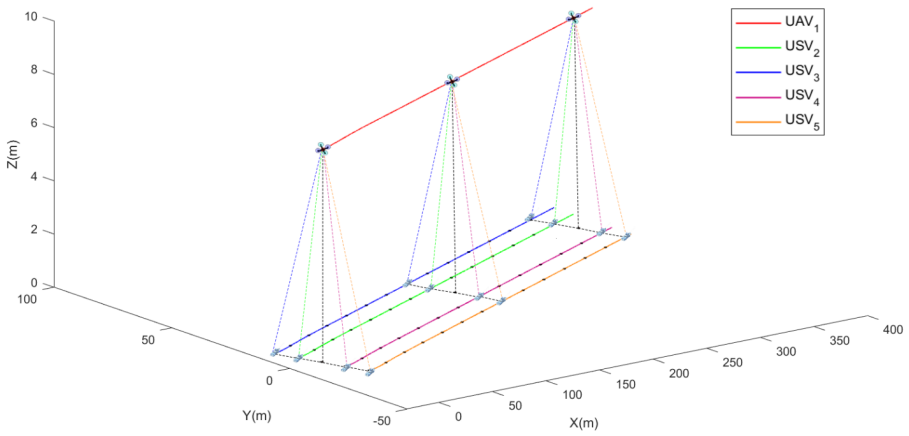

Figure 3. Motion model of USVs and UAV in case 1.

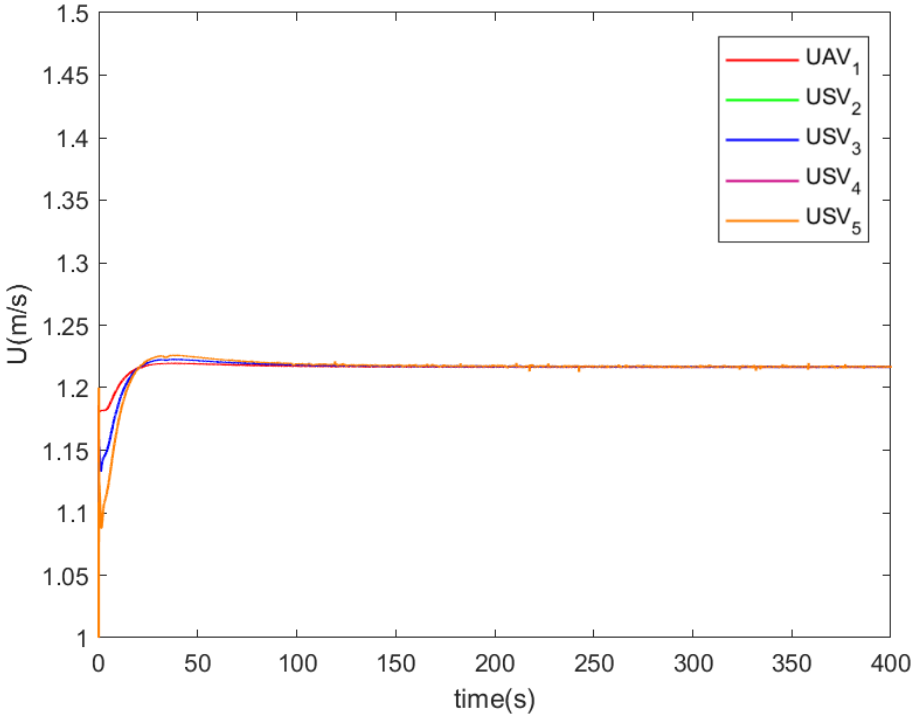

Figure 4. Longitudinal velocity of USVs and UAV.

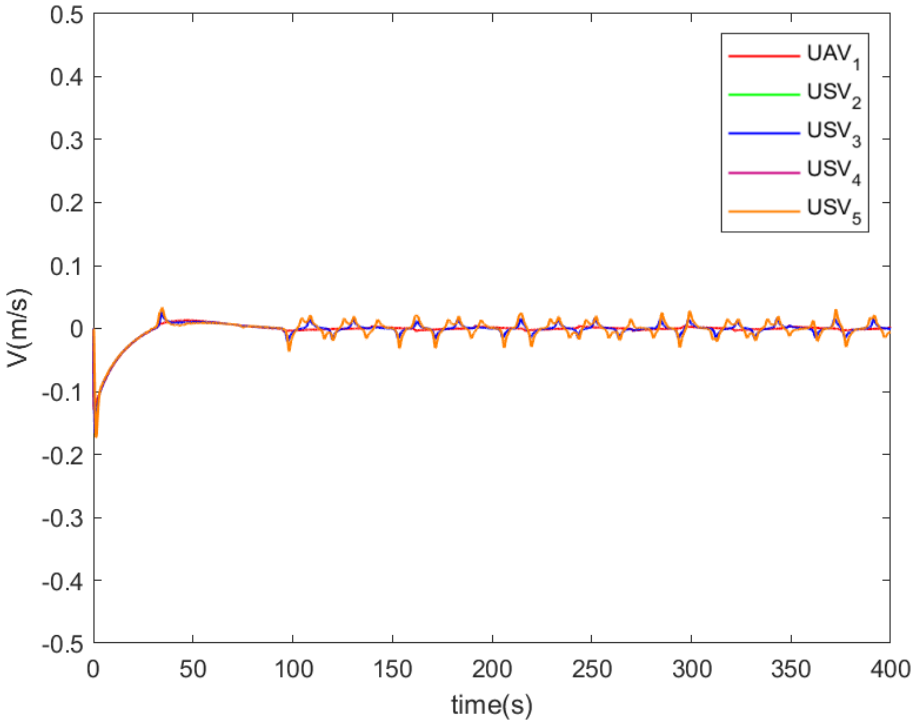

Figure 5. Lateral velocity of USVs and UAV.

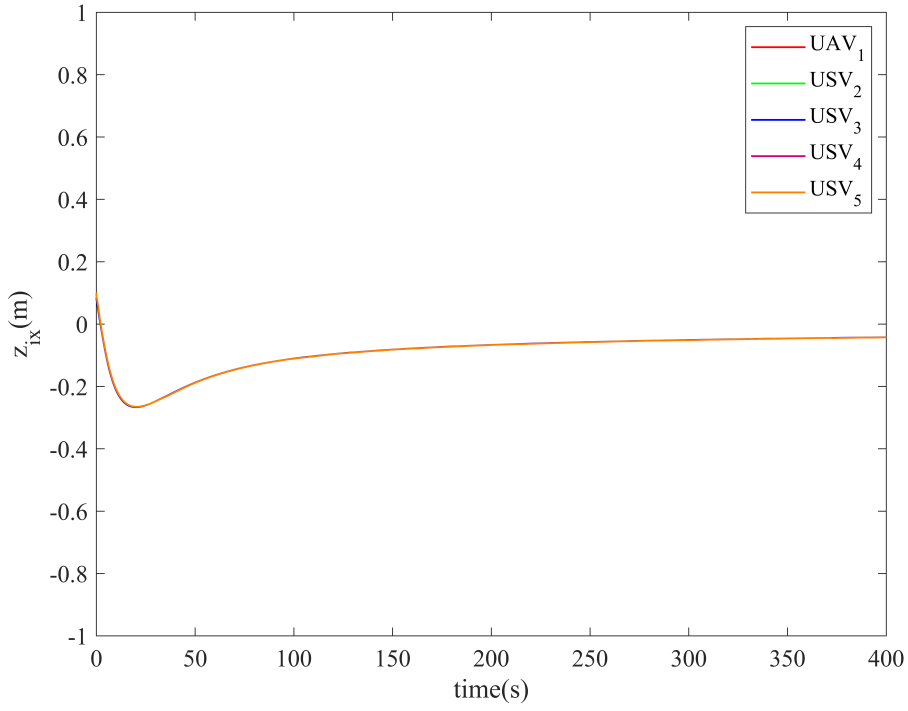

Figure 6. Longitudinal formation tracking errors.

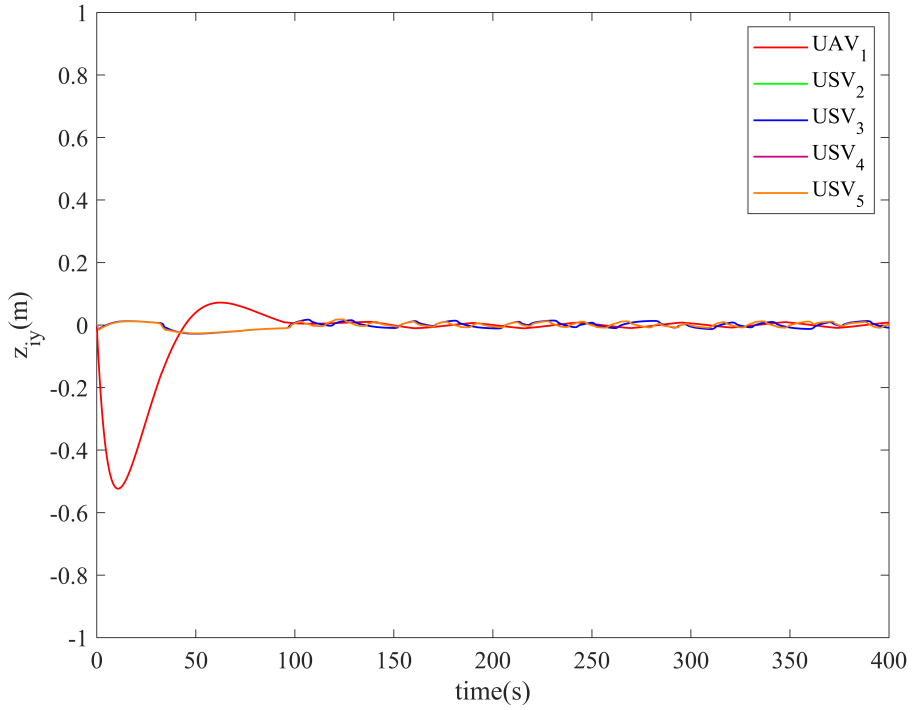

Figure 7. Lateral formation tracking errors.

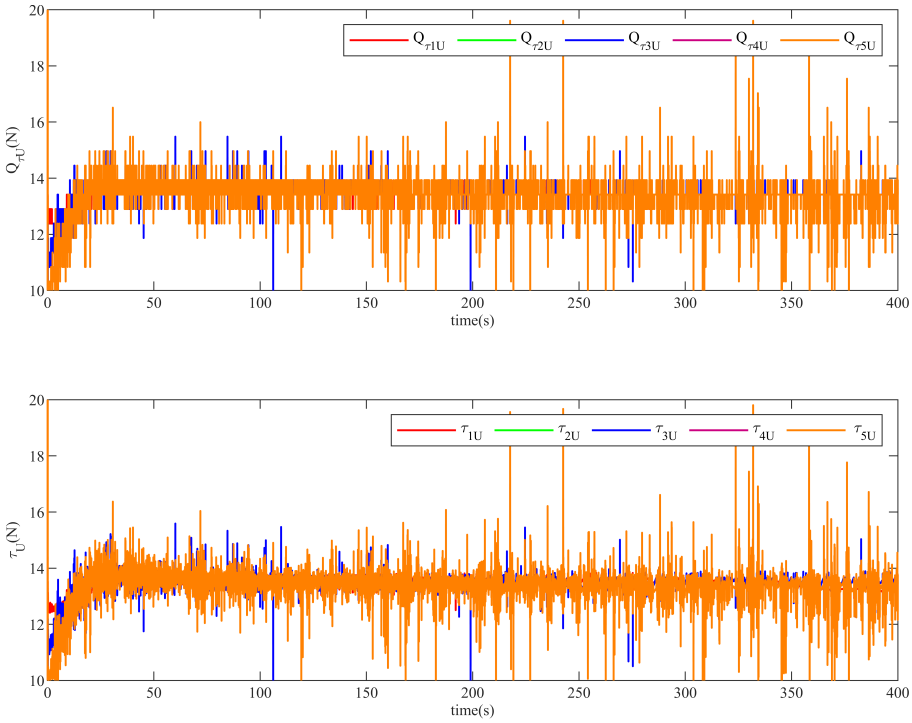

Figure 8. Comparison of longitudinal control inputs.

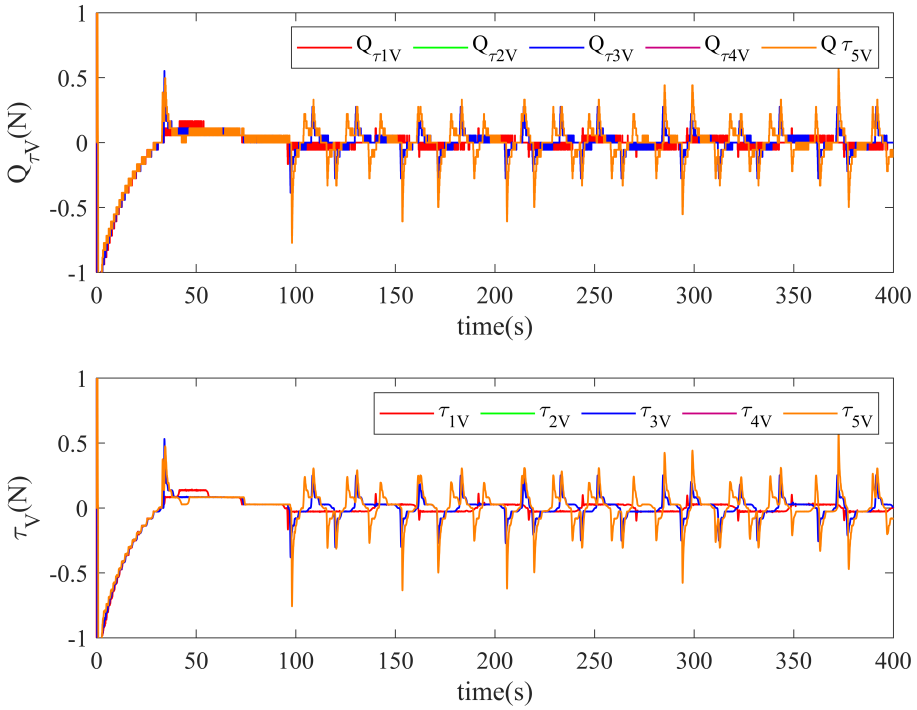

Figure 9. Comparison of lateral control inputs.

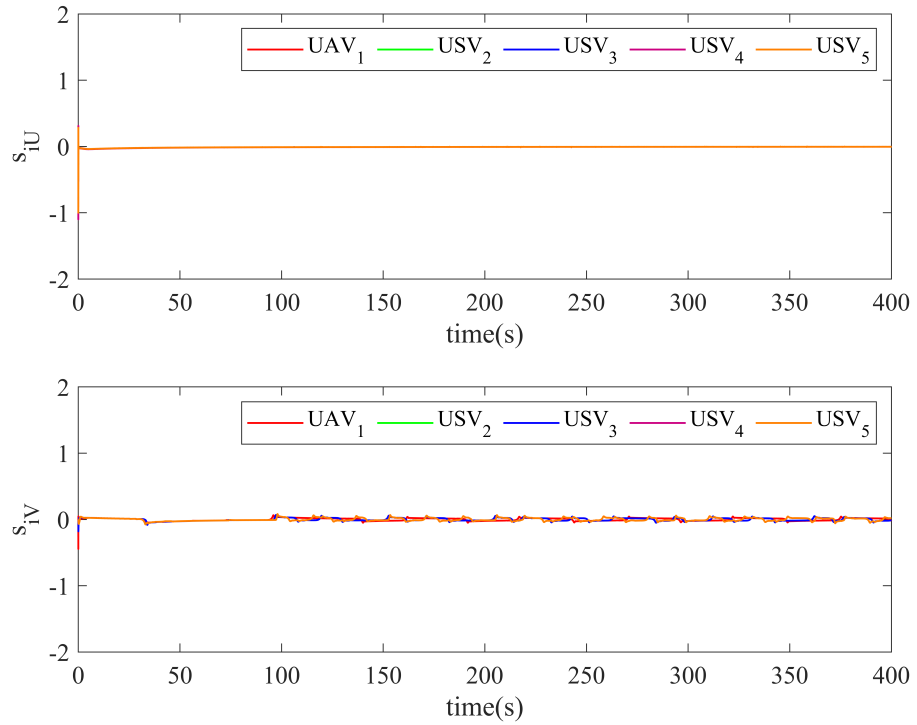

Figure 10. Sliding mode function of USVs and UAV.

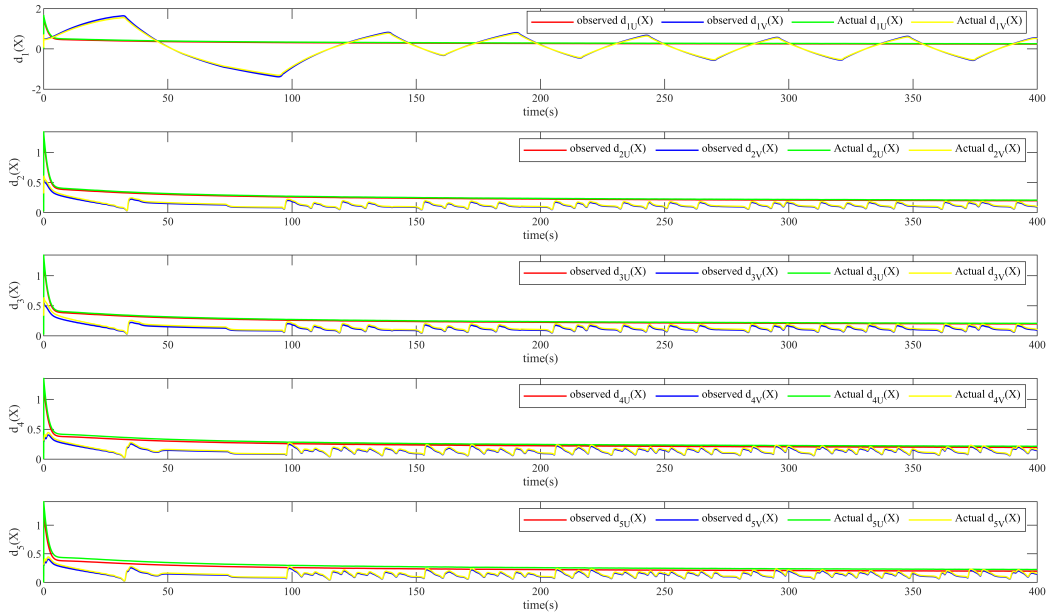

Figure 11. Estimated performance of ESO.

Case 2. To further discuss the effectiveness of the proposed controller, we compare the proposed quantization controller with the strategy proposed in [27,45,46]. Let leader UAV navigate along the reference trajectory $p_0 = [0.2t, 2\sin 0.1t - 3]^T$. The other initial conditions and control design parameters are chosen the same as their counterparts in Case 1.

The simulation results are presented in Figures 12–16. Figure 12 shows the formation trajectories of the five HMAS. As can be seen from the figure, in the XY plane the five HMAS set off from a given initial position, maintain the desired distance from each other, and maintain a special formation under the influence of external interference and system internal error. Figures 13 and 14 depict the comparison curve of longitudinal control input $Q(\tau_U(t))$ and lateral control input $Q(\tau_V(t))$ in different methods, respectively. Figures 15 and 16 present the longitudinal and lateral formation tracking error comparisons between the two control strategies, respectively. The analysis of these figures reveals that the implementation of a linear time-varying model for representing the quantizers leads to reduced tracking errors in the proposed control strategy, thereby enhancing its tracking accuracy.

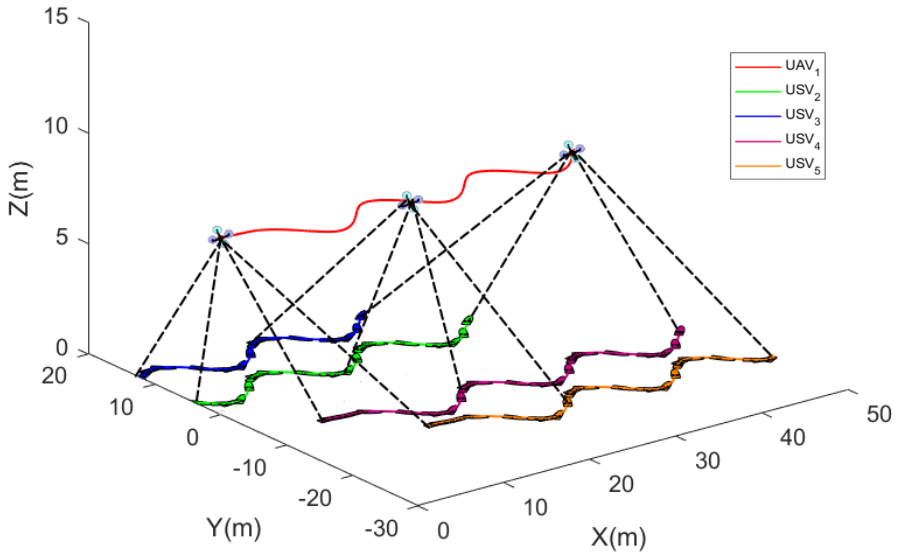

Figure 12. Motion model of USVs and UAV in case 2.

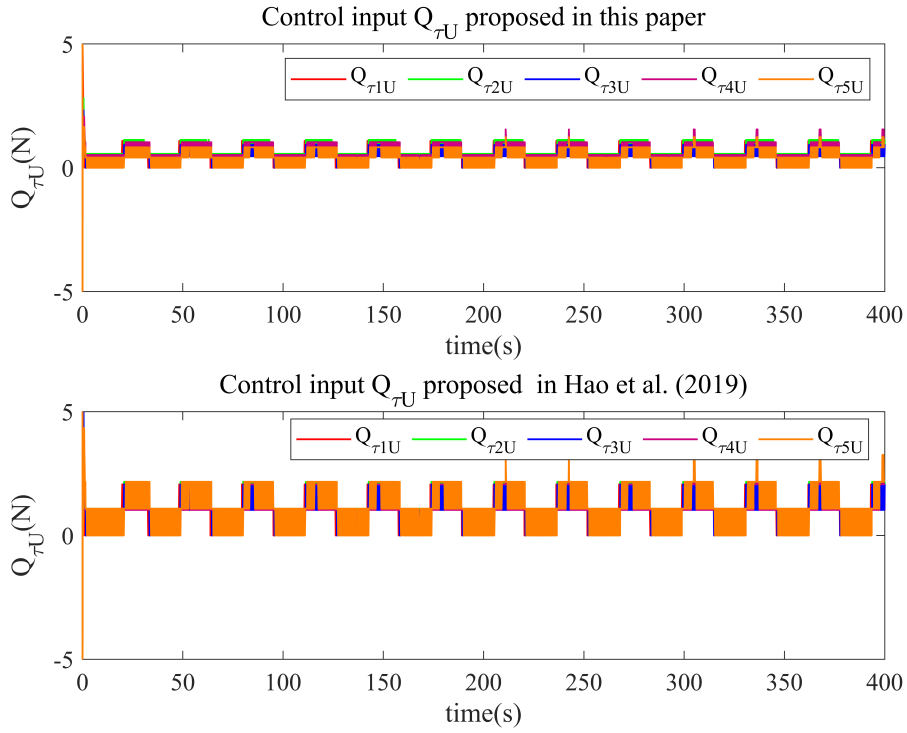

Figure 13. Comparison of longitudinal control inputs.

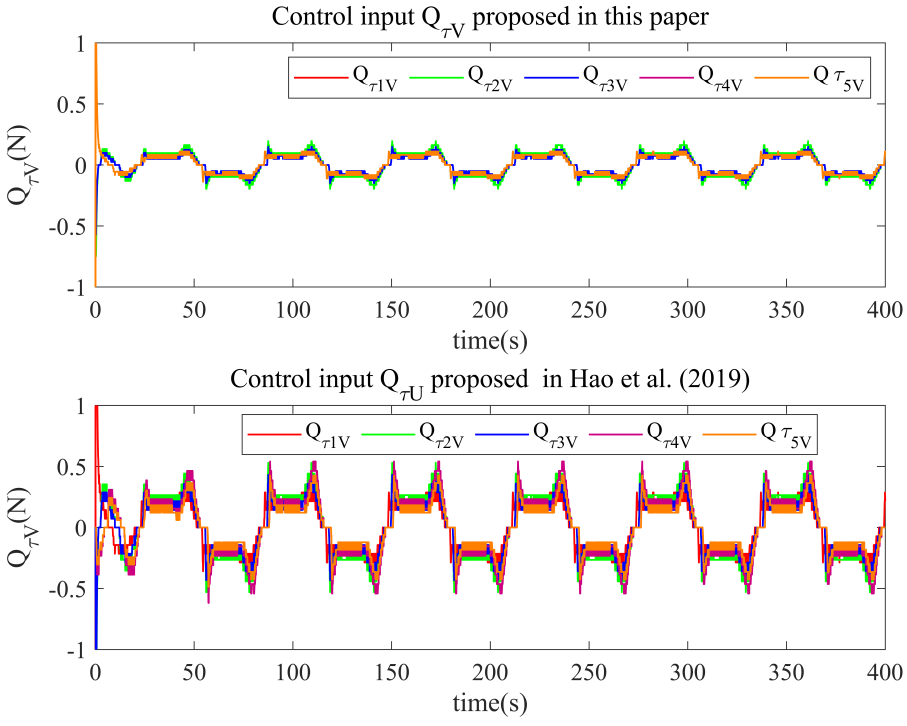

Figure 14. Comparison of lateral control inputs.

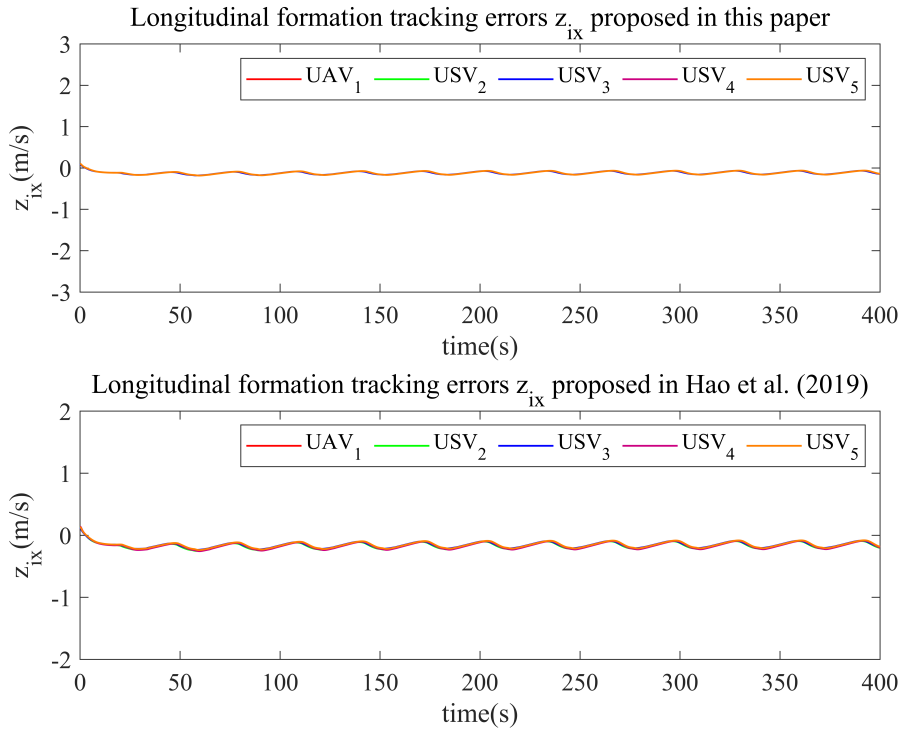

Figure 15. Comparison of longitudinal formation tracking errors.

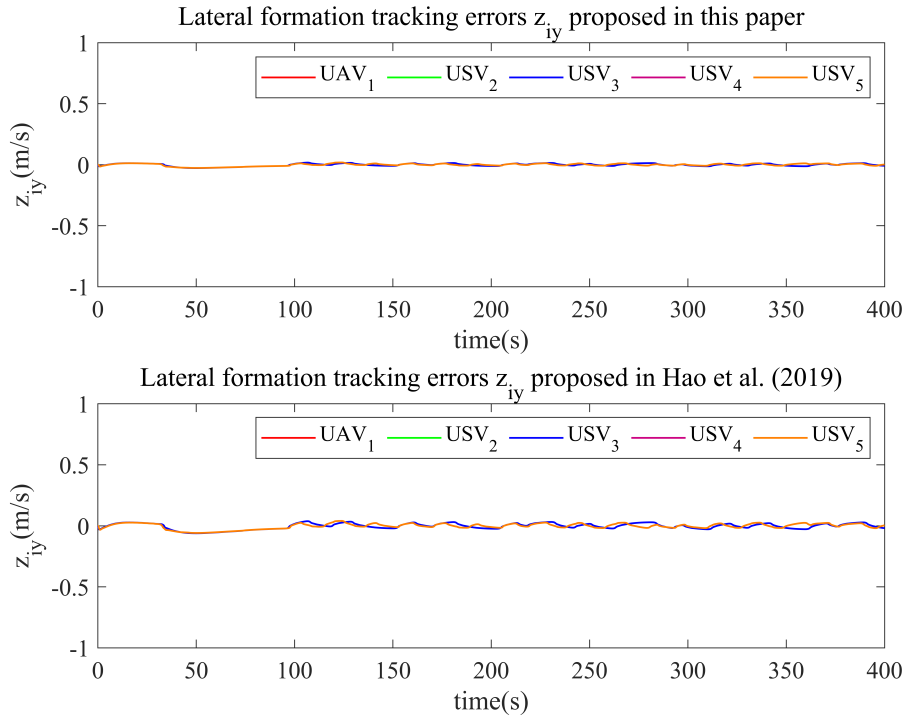

Figure 16. Comparison of lateral formation tracking errors.

6. Conclusions

This paper outlines a distributed time-varying formation control framework tailored for USVs and UAVs. The process commences with the unification of the heterogeneous agent models for UAVs and USVs, Subsequently, a trajectory-guidance law incorporating ESO considerations is devised, enabling the pursuit of time-varying trajectories on the XY plane. Within the dynamic subsystems, ESO mechanisms are harnessed to identify

unknown system functions, facilitating the development of linear time-varying models that aptly characterize quantizers. Remarkably, this approach obviates the necessity for quantizer parameter information. The closed-loop system's input-state stability is rigorously demonstrated, affirming the system's robust performance. In culmination, the efficacy of the proposed adaptive distributed formation tracking controller is rigorously verified through comprehensive simulation results.

The scope of this paper is currently limited to the heterogeneous formation consisting of a single UAV and multiple USVs. Future research should extend this work to address the cooperative dynamics of multiple UAVs and USVs in more complex scenarios. To enhance the effectiveness of the proposed algorithm, future investigations will aim to integrate transformations between formations in the presence of both dynamic and static obstacles. This integration will not only improve the algorithm's robustness but also validate its performance in terms of network lifetime and communication delay, which are crucial for real-world applications. Additionally, our future objectives include the development of methodologies to reduce communication overload and conserve communication resources within a quantized environment. By incorporating performance parameters such as network lifetime and communication delay, we aim to provide a more comprehensive evaluation of the system's effectiveness and practicality.

Author Contributions: Conceptualization, W.L. and J.N.; methodology, Y.H., Z.L., and J.N.; software, Y.H. and Z.L.; validation, Y.H.; writing—original draft preparation, Y.H. and Z.L.; writing—review and editing, Y.H., W.L., J.N., Z.L., and X.Y.; supervision, W.L. and J.N.; project administration, W.L. and Z.L.; funding acquisition, X.Y. and J.N. All authors have read and agreed to the published version of the manuscript.

Funding: This work was supported in part by the National Natural Science Foundation of China under Grants 51939001, 61976033, and in part by the Liaoning Revitalization Talents Program under Grant XLYC 1908018, XLYC 1807046, and part by the Fundamental Research Funds for the Central Universities under Grant 3132023151.

Institutional Review Board Statement: Not applicable.

Informed Consent Statement: Not applicable.

Data Availability Statement: Data are contained within the article.

Conflicts of Interest: The authors declare no conflicts of interest.

References

1. Yang, Z.; Li, S.; Yu, D.; Chen, C.P. BLS-based formation control for nonlinear multi-agent systems with actuator fault and input saturation. *Nonlinear Dyn.* **2022**, *109*, 2657–2673. [CrossRef]
2. Ma, L.; Wang, Y.L.; Fei, M.R.; Pan, Q.K. Cross-dimensional formation control of second-order heterogeneous multi-agent systems. *ISA Trans.* **2022**, *127*, 188–196. [CrossRef] [PubMed]
3. Ennong, T.; Ye, L.; Teng, M.; Yulei, L.; Yueming, L.; Jian, C. Design and experiment of a sea-air heterogeneous unmanned collaborative system for rapid inspection tasks at sea. *Appl. Ocean Res.* **2024**, *143*, 103856. [CrossRef]
4. Hou, H.Q.; Liu, Y.J.; Liu, L.; Lan, J. Adaptive fuzzy formation control for heterogeneous multi-agent systems using time-varying IBLFs. *Nonlinear Dyn.* **2023**, *111*, 16077–16091. [CrossRef]
5. Mazare, M.; Asharioun, H.; Davoudi, E.; Mokhtari, M. Distributed finite-time neural network observer-based consensus tracking control of heterogeneous underwater vehicles. *Ocean Eng.* **2023**, *272*, 113882. [CrossRef]
6. Ren, H.; Ma, H.; Li, H.; Wang, Z. Adaptive Fixed-Time Control of Nonlinear MASs With Actuator Faults. *IEEE/CAA J. Autom. Sin.* **2023**, *10*, 1252–1262. [CrossRef]
7. Liu, Z.; Nojavanzadeh, D.; Saberi, A.; Stoorvogel, A.A. Scale-Free Collaborative Protocol Design for Output Synchronization of Heterogeneous Multi-Agent Systems With Nonuniform Communication Delays. *IEEE Trans. Netw. Sci. Eng.* **2022**, *9*, 2882–2894. [CrossRef]
8. Ren, H.; Cheng, Z.; Qin, J.; Lu, R. Deception attacks on event-triggered distributed consensus estimation for nonlinear systems. *Automatica* **2023**, *154*, 111100. [CrossRef]
9. Khoshnevisan, L.; Liu, X. Resilient neural network-based control of nonlinear heterogeneous multi-agent systems: a cyber-physical system approach. *Nonlinear Dyn.* **2023**, *111*, 19171–19185. [CrossRef]
10. Sun, F.; Wu, X.; Kurths, J.; Zhu, W. Group consensus of heterogeneous multi-agent systems with packet loss and unknown speed of second-order agents in cooperative–competitive networks. *Nonlinear Dyn.* **2022**, *110*, 3447–3461. [CrossRef]

11. Liu, Y.; Wang, J.; Shi, Y.; He, Z.; Liu, F.; Kong, W.; He, Y. Unmanned airboat technology and applications in environment and agriculture. *Comput. Electron. Agric.* **2022**, *197*, 106920. [CrossRef]
12. Cui, Y.; Peng, L.; Li, H. Filtered probabilistic model predictive control-based reinforcement learning for unmanned surface vehicles. *IEEE Trans. Ind. Inform.* **2022**, *18*, 6950–6961. [CrossRef]
13. Ning, J.; Ma, Y.; Liu, L.; Li, T. Fuzzy course tracking control of an unmanned surface vehicle with event-triggered mechanism and input quantization. *Ocean Eng.* **2023**, *288*, 115704. [CrossRef]
14. Mazare, M. Distributed adaptive fault tolerant formation control for multiple underwater vehicles: Free-will arbitrary time approach. *Ocean Eng.* **2023**, *286*, 115601. [CrossRef]
15. Huang, Y.; Li, W.; Ning, J.; Li, Z. Formation Control for UAV-USVs Heterogeneous System with Collision Avoidance Performance. *J. Mar. Sci. Eng.* **2023**, *11*, 2332. [CrossRef]
16. Huang, C.; Zhang, X.; Zhang, G.; Deng, Y. Robust practical fixed-time leader–follower formation control for underactuated autonomous surface vessels using event-triggered mechanism. *Ocean Eng.* **2021**, *233*, 109026. [CrossRef]
17. Li, J.; Zhang, G.; Li, B. Robust adaptive neural cooperative control for the USV-UAV based on the LVS-LVA guidance principle. *J. Mar. Sci. Eng.* **2022**, *10*, 51. [CrossRef]
18. Tan, G.; Zhuang, J.; Zou, J.; Wan, L. Coordination control for multiple unmanned surface vehicles using hybrid behavior-based method. *Ocean Eng.* **2021**, *232*, 109147. [CrossRef]
19. Huang, D.; Li, H.; Li, X. Formation of Generic UAVs-USVs System Under Distributed Model Predictive Control Scheme. *IEEE Trans. Circuits Syst. II Express Briefs* **2020**, *67*, 3123–3127. [CrossRef]
20. Xue, K.; Wu, T. Distributed consensus of USVs under heterogeneous UAV-USV multi-agent systems cooperative control scheme. *J. Mar. Sci. Eng.* **2021**, *9*, 1314. [CrossRef]
21. Liu, H.; Weng, P.; Tian, X.; Mai, Q. Distributed adaptive fixed-time formation control for UAV-USV heterogeneous multi-agent systems. *Ocean Eng.* **2023**, *267*, 113240. [CrossRef]
22. Li, S.; Wang, X.; Wang, S.; Zhang, Y. Distributed Bearing-Only Formation Control for UAV-UWSV Heterogeneous System. *Drones* **2023**, *7*, 124. [CrossRef]
23. Liu, S.; Jiang, B.; Mao, Z.; Ma, Y. Adaptive Fault-Tolerant Formation Control of Heterogeneous Multi-Agent Systems under Directed Communication Topology. *Sensors* **2022**, *22*, 6212. [CrossRef] [PubMed]
24. Li, H.; Li, X. Distributed consensus of heterogeneous linear time-varying systems on UAVs–USVs coordination. *IEEE Trans. Circuits Syst. II Express Briefs* **2019**, *67*, 1264–1268. [CrossRef]
25. Hao, L.Y.; Yang, G.H. Robust fault tolerant control based on sliding mode method for uncertain linear systems with quantization. *ISA Trans.* **2013**, *52*, 600–610. [CrossRef] [PubMed]
26. Hao, L.Y.; Zhang, H.; Li, H.; Li, T.S. Sliding mode fault-tolerant control for unmanned marine vehicles with signal quantization and time-delay. *Ocean Eng.* **2020**, *215*, 107882. [CrossRef]
27. Hao, L.Y.; Zhang, H.; Guo, G.; Li, H. Quantized sliding mode control of unmanned marine vehicles: Various thruster faults tolerated with a unified model. *IEEE Trans. Syst. Man Cybern. Syst.* **2019**, *51*, 2012–2026. [CrossRef]
28. Hayakawa, T.; Ishii, H.; Tsumura, K. Adaptive quantized control for linear uncertain discrete-time systems. *Automatica* **2009**, *45*, 692–700. [CrossRef]
29. Wang, C.; Wen, C.; Lin, Y.; Wang, W. Decentralized adaptive tracking control for a class of interconnected nonlinear systems with input quantization. *Automatica* **2017**, *81*, 359–368. [CrossRef]
30. Xiong, S.; Wu, Q.; Wang, Y. Distributed Coordination of Heterogeneous Multi-agent Systems with Dynamic Quantization and L 2- L Control. *Int. J. Control Autom. Syst.* **2020**, *18*, 2468–2481. [CrossRef]
31. Zheng, B.C.; Yang, G.H. Quantized output feedback stabilization of uncertain systems with input nonlinearities via sliding mode control. *Int. J. Robust Nonlinear Control* **2014**, *24*, 228–246. [CrossRef]
32. Choi, Y.H.; Yoo, S.J. Distributed quantized feedback design strategy for adaptive consensus tracking of uncertain strict-feedback nonlinear multiagent systems with state quantizers. *IEEE Trans. Cybern.* **2021**, *52*, 7069–7083. [CrossRef] [PubMed]
33. Fang, X.; Zhou, J.; Wen, G. Location game of multiple unmanned surface vessels with quantized communications. *IEEE Trans. Circuits Syst. II Express Briefs* **2021**, *69*, 1322–1326. [CrossRef]
34. Salam, A.; Javaid, Q.; Ahmad, M.; Wahid, I.; Arafat, M.Y. Cluster-Based Data Aggregation in Flying Sensor Networks Enabled Internet of Things. *Future Internet* **2023**, *15*, 279. [CrossRef]
35. Liu, H.; Meng, Q.; Peng, F.; Lewis, F.L. Heterogeneous formation control of multiple UAVs with limited-input leader via reinforcement learning. *Neurocomputing* **2020**, *412*, 63–71. [CrossRef]
36. Alam, M.M.; Arafat, M.Y.; Moh, S.; Shen, J. Topology control algorithms in multi-unmanned aerial vehicle networks: An extensive survey. *J. Netw. Comput. Appl.* **2022**, *207*, 103495. [CrossRef]
37. Cheng, W.; Zhang, K.; Jiang, B.; Simani, S. Neural Network Observer-Based Prescribed-Time Fault-Tolerant Tracking Control for Heterogeneous Multiagent Systems With a Leader of Unknown Disturbances. *IEEE Trans. Aerosp. Electron. Syst.* **2023**, *59*, 9042–9053. [CrossRef]
38. Lv, C.; Chen, J.; Yu, H.; Chi, J.; Yang, Z. Adaptive NN state error PCH trajectory tracking control for unmanned surface vessel with uncertainties and input saturation. *Asian J. Control* **2023**, *25*, 3903–3919. [CrossRef]
39. Huang, T.; Chen, Z.; Gao, W.; Xue, Z.; Liu, Y. A USV-UAV Cooperative Trajectory Planning Algorithm with Hull Dynamic Constraints. *Sensors* **2023**, *23*, 1845. [CrossRef]

40. Wang, N.; Ahn, C.K. Coordinated trajectory-tracking control of a marine aerial-surface heterogeneous system. *IEEE/ASME Trans. Mechatron.* **2021**, *26*, 3198–3210. [CrossRef]
41. Li, J.; Zhang, G.; Shan, Q.; Zhang, W. A novel cooperative design for USV-UAV systems: 3D mapping guidance and adaptive fuzzy control. *IEEE Trans. Control Netw. Syst.* **2023**, 10, 564–574. [CrossRef]
42. Chen, F.; Jiang, R.; Zhang, K.; Jiang, B.; Tao, G. Robust backstepping sliding-mode control and observer-based fault estimation for a quadrotor UAV. *IEEE Trans. Ind. Electron.* **2016**, *63*, 5044–5056. [CrossRef]
43. Park, B.S.; Kwon, J.W.; Kim, H. Neural network-based output feedback control for reference tracking of underactuated surface vessels. *Automatica* **2017**, *77*, 353–359. [CrossRef]
44. Sontag, E.D.; Wang, Y. On characterizations of the input-to-state stability property. *Syst. Control Lett.* **1995**, *24*, 351–359. [CrossRef]
45. Hao, L.Y.; Zhao, Z.H. Quantized Sliding Mode Fault-Tolerant Control for Unmanned Marine Vehicles with Thruster Saturation. *J. Mar. Sci. Eng.* **2023**, *11*, 309. [CrossRef]
46. Hao, L.Y.; Yu, Y.; Li, T.S.; Li, H. Quantized output-feedback control for unmanned marine vehicles with thruster faults via sliding-mode technique. *IEEE Trans. Cybern.* **2021**, *52*, 9363–9376. [CrossRef]

Disclaimer/Publisher's Note: The statements, opinions and data contained in all publications are solely those of the individual author(s) and contributor(s) and not of MDPI and/or the editor(s). MDPI and/or the editor(s) disclaim responsibility for any injury to people or property resulting from any ideas, methods, instructions or products referred to in the content.